TURUN YLIOPISTON JULKAISUJA
ANNALES UNIVERSITATIS TURKUENSIS

SARJA - SER. A I OSA - TOM. 455

ASTRONOMICA - CHEMICA - PHYSICA - MATHEMATICA

PERTURBATIVE AND NON-PERTURBATIVE STUDIES OF REHEATING IN THE CURVATON SCENARIO

by

Jani Sainio

TURUN YLIOPISTO
UNIVERSITY OF TURKU
Turku 2013

From

Department of Physics and Astronomy
University of Turku
Finland

Supervised by

Iiro Vilja
University lecturer
Docent of Theoretical Physics
Department of Physics and Astronomy
University of Turku
Finland

Tuomas Multamäki
Docent of Theoretical Physics
Department of Physics and Astronomy
University of Turku
Finland

Reviewed by

Andrei Frolov
Associate Professor
Department of Physics
Simon Fraser University
Canada

Hannu Kurki-Suonio
University lecturer
Department of Physics
University of Helsinki
Finland

Opponent

Antonio Riotto
Professor
Department of Theoretical Physics
Geneva Cosmology and Astroparticle Group and
Centre for Astroparticle Physics
University of Geneva
Switzerland

ISBN 978-951-29-5282-3 (PRINT)
ISBN 978-951-29-5283-0 (PDF)
ISSN 0082-7002
Painosalama - Turku, Finland 2013

'From the moment I picked your book up until I laid it down, I convulsed with laughter. Someday I intend on reading it.'

- **Groucho Marx**

Acknowledgements

As this thesis is inevitably an ending to a rather long endeavour it might be a good idea to look back where it all started. The author's first foray into the field of science was an "entry" into a Finnish science competition, Viksu, with a wildly "fascinating" rambling on black holes. As I now re-read that "study" I see that the use of words "reviewer hospitalized", "losing faith in humanity" and "excessive loss of precious bodily fluids" in the feedback that I received were not entirely out of place. Obviously somehow something went terribly wrong in that essay.

If the reading of this thesis causes none of the aforementioned symptoms it is all because of my supervisors, University Lecturer Iiro Vilja and Docent Tuomas Multamäki, who have forged and shaped me in the last few years. During this time I have often entered Iiro's chamber thinking "Help me Iiro Vilja. You're my only hope." Within a minute or two not only would he do the work that took me often weeks to accomplish but also show me what I'd done wrong. Therefore if anyone reading this has any mathematical problems no matter how difficult I'm sure Iiro will be able to solve them in a breeze. His guidance was equally important when the research articles and the introduction to this thesis were written.

Contributions by Tuomas Multamäki were also crucial for the success of this project, especially for helping me improve my scientific writing skills, providing funding in the first years through different projects of the Academy of Finland, teaching the often neglected art of being Quick-And-Dirty and for introducing me to the interesting research area of quantitative finance. And lastly, for teaching me the mantra "don't think, just do it" which I have tried to apply to the best of my knowledge to this thesis.

A good journey also always needs a helping hand in the form of financial support. The first years were supported by project Nos. 8111953 and 8129850 of the Academy of Finland. After this Professor Luis Alvarez made me "an offer I couldn't refuse" and hired me for a year and a half to the Turku School of Economics to work on issues related to quantitative finance

on a project funded by OP Bank Group Research Foundation. While there I was also thankfully able to pursue the research that was needed in the latter part of the thesis. Lastly, the writing of this introduction was financed by University of Turku Grant for Completing a Doctoral Degree and by the Kauko Mansikka memorial fund granted by Turku University Foundation.

The pre-examiners of this thesis, Associate Professor Andrei Frolov and University Lecturer Hannu Kurki-Suonio, and the language examiner, Docent Chris Flynn, are gratefully acknowledged for giving very useful and insightful comments on the manuscript that helped improve it greatly. I am also grateful that Professor Antonio Riotto has agreed to be my opponent. His research, especially on the subject of non-Gaussianity, has been very influential on the studies done in this thesis.

Majority of this work was done at the Laboratory of Theoretical Physics which provided an inspiring atmosphere to not only learn new things about physics and life but also to attain various other skills that might prove to be useful someday, including the secrets of human appendix removal (appendectomy). One year was also spent at Tuorla observatory where the seeds of the last part of this thesis were planted.

In addition I would like to thank those who had more implicit role in the making of this thesis: family, relatives, friends and colleagues (real and/or imaginary), the wonderful producers of Nexium, Cetirizine and Panadol medicines and finally my gods/heroes, Johnny Cash, The Edge, David Gilmour, Jimi Hendrix and Neil Young. Last but not least I would like to thank Line 6, Blondie (not the band), Blackie Jr. III and Sunnie for making this improbable journey on this third stone from the Sun sonically so much more interesting.

'Come... dry your eyes. For you are life, rarer than a quark and unpredictable beyond the dreams of Heisenberg; the clay in which the forces that shape all things leave their fingerprints most clearly.'

- **Dr. Manhattan** in Alan Moore's *Watchmen*

Contents

Abstract

Reheating is an important part of the evolution of the early Universe: it is needed to restore the radiation dominated conditions of the Big Bang era after cosmic inflation has ended. In this thesis this reheating process has been studied with perturbative and non-perturbative methods in the curvaton scenario, a well motivated alternative to the standard inflation paradigm. The aim of these studies has been to determine the level of the produced non-Gaussianity which can be compared to the limits given by cosmic microwave background radiation. In addition the physicality of the curvaton scenario has been investigate in terms of the temperature limits given by standard cosmology.

In the perturbative case different variants of a three fluid model were studied where the curvaton is assumed to decay into both radiation and cold-dark matter. Parts of the studied parameter space that lead to temperatures within the limits given by standard cosmology were identified. The level of non-Gaussianity was generally found to be small if the curvaton is also responsible for the generation of the cold-dark matter component of the Universe.

In the non-perturbative reheating scenario a self-interacting curvaton model was studied with emphasis on the level of non-Gaussianity generated. To calculate this quantity, two groundbreaking computational programs were developed that use graphics processing units (GPUs) to accelerate the numerical computations significantly. In addition a symplectic integrator was implemented in the latter of the codes to improve the accurate considerably. As a result, the evolution during different preheating scenarios can be now computed significantly faster using inexpensive common desktop computers without needing to sacrifice accuracy. The level of non-Gaussianity in the self-interacting curvaton model was found to be quite large and inconsistent with current observational limits, in line with previous results from other preheating scenarios.

List of papers

This thesis consist of the introductory review part and the following research papers [1–6]:

I T. Multamäki, J. Sainio, and I. Vilja, *Constraints on the three-fluid model of curvaton decay*, Int. J. Mod. Phys. D**18** (2009) 2047–2059, [arXiv:0710.0282].

II T. Multamäki, J. Sainio, and I. Vilja, *Non-Gaussianity in three fluid curvaton model*, Phys. Rev. D**79** (2009) 103516, [arXiv:0803.2637].

III J. Sainio and I. Vilja, *Curvaton decay into relativistic matter*, Phys. Rev. D**81** (2010) 083516, [arXiv:0912.3394].

IV J. Sainio, *CUDAEASY - a GPU Accelerated Cosmological Lattice Program*, Comput. Phys. Commun. **181** (2010) 906–912, [arXiv:0911.5692].

V J. Sainio, *PyCOOL - a Cosmological Object-Oriented Lattice code written in Python*, JCAP **1204** (2012) 038, [arXiv:1201.5029].

VI J. Sainio, *Curvaton preheating revisited*, Phys. Rev. D**85** (2012) 123515, [arXiv:1203.5316].

Chapter 1

Introduction

Writing a symphony on the birth and development of the Universe might seem like a daunting task. To describe the fiery furnace in which the Cosmos was born, the first movement would have to be very fast and almost deafening loud. This intense period would, however, last only for a short period of time after which the volume and pace would need to be turned down considerably to illustrate the rather rapid cooling of the Universe. The second movement would have to describe the next, much more peaceful and longer epoch during which cosmic structures start to develop forming eventually stars, galaxies and galaxy clusters. This part would ultimately end with the present day Universe followed by a final movement expressing the murky future of the Cosmos.

Historically there have been numerous religious or mythical compositions of this cosmic symphony. In contrast to these, the one provided by modern cosmology is written in the language of mathematics and is based firmly on results from different astrophysical observations and particle physics experiments. The history of modern cosmology can be said to start from the publication of general relativity [7] that made it possible to formulate a mathematically consistent model for the evolution of the Universe. Since then physical cosmology has evolved significantly with improved observational programs that include Edwin Hubble's measurements of distant galaxies [8] in 1929 to the more recent observations of the cosmic microwave background (CMB) radiation [9–11].

Nowadays it is widely believed that the early Universe experienced a period of cosmic inflation during which it expanded at a phenomenal rate. The original motion for this was in solving various problems of the standard cosmology [12–16] although it was soon noticed [17–19] that it can also

explain the origin of the cosmic structures we see today, *e.g.* galaxies and galaxy groups, by creating small density fluctuations in the Universe.

In the simplest inflationary paradigm these both functions are handled by a single scalar field, called inflaton. A well motivated alternative to this description is the curvaton scenario where the cosmological perturbations are assumed to originate from a scalar field that is not responsible for the expansion of space. As a consequence the inflation model is liberated from the constraint to produce the observed CMB amplitude which makes the construction of different inflaton models easier [20].

In this thesis we will concentrate on two vastly different models for the curvaton scenario. In the first three research articles [1–3] we study variations of a curvaton model where the curvaton field decays into radiation and cold dark matter. In these studies we seek regions of parameter space where the solutions lead to evolution consistent with the thermal history of the Universe. We then concentrate on a non-perturbative decay mechanism in the curvaton scenario. To this end we develop two cutting-edge computational programs that use graphics processing units (GPUs) to accelerate the numerical computations drastically. These codes are presented in research articles [4, 5]. In the final research paper [6] we will apply the computational methods to a model where a self-interacting curvaton field decays through a violent and rapid preheating process.

The main objective is essentially the same in these two cases: the study of how much the distribution of the cosmological perturbations deviates from a Gaussian one. This study of non-Gaussianity has been a popular subject in cosmology [21] in the last ten years due to new and improved observational programs that have been able to measure the statistics of the small perturbations from the CMB radiation [10, 11] with unprecedented accuracy. The level of non-Gaussianity depends greatly on the used model [21] and can therefore provide a valuable method to separate physically viable models from those that are in conflict with the observations.

The introductory review part is organized as follows: in Chapter 2 we discuss the basics of the early universe, namely Friedmann-Robertson-Walker solutions of the Einstein equations, the period of cosmic inflation and the reheating of the Universe. In Chapter 3 we review the basics of cosmological perturbation theory as is relevant to this thesis. Chapter 4 introduces the computational techniques and methods we have developed and used in the thesis. In Chapter 5 different variants of non-Gaussianity are presented in the perturbative and non-perturbative cases. We conclude with a summary of the research papers and an outlook on the subjects we

have discussed.

Notation

We use natural units in this thesis where we set $\hbar = c = k_{\mathrm{B}} = 1$. In addition we also set the reduced Planck mass $m_{\mathrm{Pl}} = 1/\sqrt{8\pi G}$ to unity in most of the research articles.

Chapter 2

The early Universe

Modern cosmology is build on the theoretical foundation of general relativity [7] which determines the evolution of the Universe given its energy content. In this chapter we present the main concepts of the general relativity and the early Universe as is relevant to this thesis.

2.1 Friedmann-Robertson-Walker cosmology

The cosmological principle is a central premise of modern cosmology. It states that on large scales the Universe 'looks the same whoever and wherever you are.'[22] More specifically it states that the Universe is spatially homogeneous and isotropic meaning that observers at different locations will see it similarly in all directions. This assumption is supported by current cosmological observations, most significantly different mappings of the cosmic microwave background radiation (CMB) [23–25] that show that the temperature was very homogeneous and isotropic when the Universe was roughly 380 000 years old.

In general relativity the central object of study is the metric tensor, $g_{\mu\nu}$, which carries vital information on the structure of spacetime. In a spatially isotropic and homogeneous universe it is given by the Friedmann-Robertson-Walker metric [26]

$$ds^2 = dt^2 - a(t)^2\left(\frac{dr^2}{1-Kr^2} + r^2 d\theta^2 + r^2 \sin^2\theta\, d\phi^2\right), \tag{2.1}$$

where t is the coordinate time, r, θ and ϕ are the polar coordinates, $a(t)$ is the scale factor and $K \in \{-1, 0, 1\}$ is the curvature of the universe. In

this thesis we will be interested mostly in flat universes with $K = 0$ which is supported by CMB observations [25]. The metric (2.1) then simplifies to

$$ds^2 = dt^2 - a(t)^2 dx^i dx^i \tag{2.2}$$

where summation is done over the i index and dx^i are the comoving spatial coordinates.

The relevant equations of motion are given by the Einstein field equations [7, 27]

$$R_{\mu\nu} - \frac{1}{2} R g_{\mu\nu} = -8\pi G T_{\mu\nu} \tag{2.3}$$

which tell how the curvature of the spacetime, on the left-hand side, and its energy content, on the right-hand side, are intertwined. Here $R_{\mu\nu}$ is the Ricci tensor, R the Ricci scalar and G is Newton's gravitational constant. The stress-energy tensor, $T_{\mu\nu}$, that describes the matter content of the Universe has to have the same symmetries as the metric tensor $g_{\mu\nu}$ [28]. In a Robertson-Walker universe this means that it is of the isotropic perfect fluid type for which

$$T^\nu_\mu = (\rho + P) u_\mu u^\nu - P \delta^\nu_\mu, \tag{2.4}$$

where ρ is the energy density in a local rest frame, P the pressure and u_ν is the 4-velocity of the fluid. Contracting both sides of Eq. (2.3) with the covariant derivative, D_μ, gives the continuity equation

$$D_\mu T^{\mu\nu} = 0, \tag{2.5}$$

which gives the evolution of the fluid energy density and pressure. In a Robertson-Walker universe the temporal $\nu = 0$ component gives the energy conservation law

$$\frac{\partial \rho}{\partial t} + 3\frac{\dot{a}}{a}(\rho + P) = 0 \tag{2.6}$$

whereas the spatial $\nu = i$ components are identically zero due to the form of the stress-energy tensor [29, 30].

It is usually assumed that the equation of state $\omega = P/\rho$ of the fluid is a constant and hence Equation (2.6) reads

$$\frac{\partial \rho}{\partial t} + 3\frac{\dot{a}}{a}(1 + \omega)\rho = 0 \tag{2.7}$$

which can be easily solved to give

$$\rho \propto a^{-3(1+\omega)}. \tag{2.8}$$

There are three special cases that are often encountered in cosmology: non-relativistic dust $\omega = 0$ with $\rho \propto a^{-3}$, relativistic matter and radiation for which $\omega = 1/3$ and $\rho \propto a^{-4}$ and vacuum energy $\omega = -1$ with a constant solution ρ_Λ.

The dynamics of the Universe are now determined by the Einstein equations in combination with the continuity equation. In a Robertson-Walker universe dominated by a perfect fluid the temporal 00-component of the Einstein equations (2.3) reads [29, 30]

$$H^2 = \frac{8\pi G}{3}\rho - \frac{K}{a^2}, \tag{2.9}$$

where $H = \dot{a}/a$ is the Hubble parameter in physical time and K is the curvature of the Universe. This is the first Friedmann equation and is often written in terms of the critical energy density

$$\rho_\mathrm{c} = \frac{3H^2}{8\pi G} \tag{2.10}$$

as

$$\frac{K}{a^2} = H^2(\Omega - 1), \tag{2.11}$$

where we have also defined the fractional energy density

$$\Omega = \frac{\rho}{\rho_\mathrm{c}}. \tag{2.12}$$

Equation (2.11) shows explicitly the relationship between the sign of the curvature and the critical energy density. For $\Omega > 1$ the curvature K is positive, which corresponds to a closed universe whereas for $\Omega < 1$ K is negative and the universe is open. Currently the most interesting possibility, however, is a flat cosmos with $\Omega = 1$ which is in best agreement with the recent cosmological observations [25]. The second Friedmann equation is given by the spatial part of the Einstein equations and it reads

$$\frac{\ddot{a}}{a} = -\frac{4\pi G}{3}(3p + \rho). \tag{2.13}$$

The evolution of the Universe can be solved rather easily for matter, radiation and vacuum dominated universes by integrating the first Friedmann equation. The scale factors read in terms of the physical time $a(t) \propto t^{2/3}$, $a(t) \propto t^{1/2}$ and $a \propto \exp H_0 t$, respectively, where H_0 is the (constant) Hubble parameter. The last of these solutions is called the de Sitter universe which

will be very import when discussing cosmic inflation.

Note these equations have been derived in terms of the physical time t. It is customary to define the conformal time η as $dt = ad\eta$ which simplifies the line element (2.2) into the form

$$ds^2 = a(\eta)^2(d\eta^2 - dx^i dx^i). \tag{2.14}$$

The Friedmann equations then read

$$\begin{aligned} \mathcal{H}^2 &= \frac{8\pi G}{3}a^2\rho - K, \\ a'' &= -\frac{4\pi G}{3}(3p - \rho)a^3, \end{aligned} \tag{2.15}$$

where $\mathcal{H} = a'/a$ is the Hubble parameter in conformal time. As an example, for a flat de Sitter space with constant Hubble parameter H, the first Friedmann equation can be written as

$$\frac{a'(\eta)}{a(\eta)^2} = H \tag{2.16}$$

from which it follows that

$$a(\eta) = -\frac{1}{H\eta}, \tag{2.17}$$

where the conformal time goes from $-\infty$ to 0.

2.2 Cosmic horizons

The Hubble parameter $H = \dot{a}/a$ is an import quantity in cosmology. Besides measuring the expansion rate of the Universe it also gives a characteristic time scale of the expansion, the Hubble time, defined as H^{-1}. In a de Sitter model where the Hubble parameter is a constant and the scale factor increases exponentially the Universe expands by one e-fold in a Hubble time. A closely related concept is the Hubble distance, defined as cH^{-1}, which tells how far light travels in a Hubble time. It is customary to call this the Hubble horizon or simply the horizon. The number of e-foldings between two scale factor values, a_1 and a_2, is

$$N = \ln\left(\frac{a_2}{a_1}\right) = \int_{t_1}^{t_2} H dt \tag{2.18}$$

and hence measures the number of Hubble times. Note that in some of the papers in this thesis we write the equations of motion in terms of the number of e-folds, N.

Other interesting distance measures are the particle and event horizons. The particle horizon is defined as the (comoving) distance light has traveled since time t_1 as

$$x_{\rm ph} = \int_{t_1}^{t} \frac{dt}{a} = \eta(t) - \eta(t_1) \tag{2.19}$$

where η is the conformal time defined previously. As no information can move faster than light, regions that are separated by a distance larger than $\eta(t)-\eta(t_1)$ could not have been in causal contact since time t_1. Usually $\eta(t_1)$ is simply set to zero to simplify the expression. The closely related event horizon is defined as the size of a region that will be causally connected in the future

$$x_{\rm eh} = \int_{t}^{t_\infty} \frac{dt}{a} = \eta(t_\infty) - \eta(t) \tag{2.20}$$

meaning that observers separated by more than the event horizon won't be able to communicate. One example of a universe with a finite event horizon is the de Sitter one.

2.3 Hot Big Bang

Different cosmological observations, most notably the Hubble diagram of distant galaxies [8], imply that the Universe is expanding. In terms of the solution of the Friedmann equations this means that the scale factor should also grow with time. Currently the simplest model in agreement with the observations is the ΛCDM model [30] that is presently dominated by an elusive dark energy ρ_Λ with a smaller contribution from a cold dark matter component, $\rho_{\rm CDM} \propto a^{-3}$. The energy density of radiation is quite small today, but because $\rho_\gamma \propto a^{-4}$ it was the dominating element of an earlier Universe. This hot and dense period is typically called the Hot Big Bang.

Most direct evidence for the radiation dominated era comes from the cosmic microwave background. The early plasma was made of frequently interacting elementary particles and photons that kept the mean-free distance traveled by radiation very short. As the Universe expanded with time, the plasma began to cool down, leading eventually to nucleosynthesis at $T \sim 0.1$ MeV. The majority of neutrons were then bound to helium-4 although a small fraction was taken by helium-3, deuterium, lithium-7 nuclei and more heavy elements [30]. As the energy density of relativistic

particles diluted more quickly than that of non-relativistic matter, the radiation dominated era eventually ended. This occurred at $T \sim 10$ eV when the Universe was roughly 10 000 years old. After this the matter component started to dominate and the scale factor began to grow more quickly, $a(t) \propto t^{2/3}$. The Universe was, however, still opaque to photons that were scattered frequently by the free electrons. This changed at $T \sim 0.1$ eV during recombination when the free electrons became bound to the nuclei to form atoms. After this the space became transparent to the photons, resulting in the production of cosmic background radiation that is observed today.

The CMB radiation is currently the primary source of information on the very early Universe. It is characterized to a very high degree by a thermal black body spectrum with the current temperature close to a value of $T = 2.725$ K [23]. It is also highly isotropic with small perturbations in the temperature at $\delta T/T \sim 10^{-5}$ level. The study of these anisotropies has been a hot topic in observational cosmology in the last decades and has provided significant amount of information on the state of the primordial Universe. Most notable observational programs are the COBE [9], WMAP [10] and Planck [11] experiments.

2.4 Inflation

Standard cosmology and the Big Bang paradigm are highly successful in explaining most of the history and the evolution of the Universe. These are, however, plagued by certain problems that are very difficult to solve without incorporating a period of cosmic inflation. The historical origin of the inflation lies in the initial conditions needed in the Big Bang model that seem to be very finely tuned to have the Universe we observe today. Nowadays its primary function is, however, the generation of cosmic perturbations [30].

One of the fine tuning issues of the standard cosmology is the flatness problem which relates to how close to the critical density the Universe was initially. From equation (2.11) we can solve

$$|\Omega - 1| = \frac{|K|}{a^2 H^2}, \tag{2.21}$$

and by assuming that the curvature K is small and that matter or radiation is dominating (*i.e.* $a \propto t^{2/3}$ or $a \propto t^{1/2}$, respectively), then $|\Omega - 1| \propto t^{2/3}$ in the matter dominated case and $|\Omega - 1| \propto t$ in the latter one. Since the Universe is currently very close to the critical density with $|\Omega - 1| < 10^{-2}$

[25] the fractional energy density, Ω, would have to be fine tuned to a very high precision in the early Universe. For example, at nucleosynthesis it is required that $|\Omega - 1| < 10^{-16}$ [30] and at earlier times, the fractional energy density must be even closer to one.

The horizon problem refers to the high level of isotropy seen in the CMB radiation. Starting from the current comoving Hubble horizon, H_0^{-1}, and by calculating it back in history, it will decrease as some power of the time variable depending on the equation of state of the Universe, as seen in the previous paragraph. The particle horizon at early times can be calculated from Eq. (2.19) and it will be generally of the same order as the comoving Hubble horizon. By going back all the way to the moment when the cosmic background radiation was produced, the comoving particle horizon was much smaller than the scales that are observed today and only small regions of it were causally connected. In essence the horizon problem then asks why these different non-causally connected regions were very homogeneous and isotropic back then.

Cosmic relics are also a cause of concern in the standard cosmology. These are exotic long-lived massive particles or other artifacts, including black holes, that are produced in the hot early cosmos in large quantities. Because their mass is generally very high, they would naturally have a significant effect on the energy density of the Universe and could make it a closed one. Since this is not the case observationally, the fractional energy density of these particles has to be somehow reduced.

Cosmic inflation is a rather elegant remedy to these problems that can at the same time explain the origin of the small anisotropies in the CMB radiation. It was first developed separately by Alan Guth, Katsuhiko Sato and Alexei Starobinsky in the early 1980's [12–14] to solve the problems of the standard cosmology. These versions of inflation were, however, found to be inadequate and improved versions were developed quickly [15, 16, 31]. Currently the so called slow-roll inflation is the most widely accepted one.

A simple definition for the period of inflation is that the expansion of the early Universe should be accelerating, *i.e.* $\ddot{a} > 0$ [30]. This is equivalent to having the comoving Hubble length decrease with time

$$\frac{d}{dt}\left(\frac{1}{aH}\right) < 0 \tag{2.22}$$

implying that regions that were interacting at the start of inflation were driven beyond the Hubble scale. Yet another form can be derived by calcu-

lating the time derivative explicitly

$$-\frac{\dot{H}}{H^2} < 1 \tag{2.23}$$

meaning that the Hubble parameter should vary slowly during inflation. The stronger version of this reads $|\dot{H}| \ll H^2$, *i.e.* H is practically a constant, and the Universe is a de Sitter one.

Assuming that the Friedmann equations are valid, the definition of inflation can be also written in terms of the energy and pressure densities from Eq. (2.13) as

$$\rho + 3p < 0 \tag{2.24}$$

meaning that equation of state of the Universe should satisfy $\omega < -\frac{1}{3}$ and the pressure of the fluid should be negative (since the energy density, ρ, is positive).

Inflation can solve the horizon and flatness problems by assuming that the observable Universe was within the Hubble horizon and only during inflation it was driven out of causal contact. The exponential increase in the scale factor also drives the critical density of the Universe very close to the critical limit. The relic problem can be partly solved since the rapid expansion of space dilutes the number density of the massive particles rather quickly. Relics produced after the inflation can, however, still pose problems [30].

2.4.1 Slow-roll inflation

We will now present the main mechanism behind the slow-roll inflation in which the inflaton field, ϕ, is assumed to slowly roll down the potential. Starting from the action of a minimally coupled scalar field in a flat Robertson-Walker universe [30]

$$S = \int \mathcal{L}_\phi \sqrt{-g}\, \mathrm{d}^4x = \int \Big(\frac{1}{2}\partial_\mu\phi\partial^\mu\phi - V(\phi)\Big)\sqrt{-g}\, \mathrm{d}^4x, \tag{2.25}$$

where $g = -a^6$ is the determinant of the metric tensor components, $g_{\mu\nu}$, the Euler-Lagrange equation of motion for the inflaton field reads

$$\ddot{\phi} + 3H\dot{\phi} - \frac{\nabla^2\phi}{a^2} + V'(\phi) = 0, \tag{2.26}$$

where prime is now derivative with respect to the field. In the homogeneous case the spatial derivative term will vanish. The stress-energy tensor for the field is [30]

$$T^{\mu\nu} = \partial^\mu\phi\partial^\nu\phi - g^{\mu\nu}\mathcal{L}_\phi \tag{2.27}$$

from which it follows that

$$\begin{aligned} \rho_\phi &= T_{00} = \frac{1}{2}\dot{\phi}^2 + \frac{\nabla^2\phi}{2a^2} + V(\phi), \\ p_\phi &= -\frac{1}{3}T_i^i = \frac{1}{2}\dot{\phi}^2 - \frac{\nabla^2\phi}{6a^2} - V(\phi). \end{aligned} \tag{2.28}$$

The first Friedmann equation then reads for the homogeneous field

$$3m_{\rm Pl}^2H^2 = \frac{1}{2}\dot{\phi}^2 + V(\phi), \tag{2.29}$$

where $m_{\rm Pl}$ is the reduced Planck mass. By taking the time derivative and using equation (2.26), we get

$$2m_{\rm Pl}^2\dot{H} = -\dot{\phi}^2. \tag{2.30}$$

If we now assume that $|\dot{H}| \ll H^2$ it follows that the kinetic terms are very small compared to the potential term which means that $p \simeq -\rho$ from equations (2.28) and the Universe is close to a de Sitter solution with the Hubble parameter having almost a constant value

$$H^2 \simeq \frac{V(\phi)}{3m_{\rm Pl}^2}. \tag{2.31}$$

By differentiating this with respect to time and using Eq. (2.30), the time derivative of the field reads

$$-3H\dot{\phi} = V'. \tag{2.32}$$

Typically it is assumed that the so called slow-roll conditions are valid. These read [30]

$$\epsilon(\phi) \equiv \frac{m_{\rm Pl}^2}{2}\Big(\frac{V'}{V}\Big)^2 \ll 1, \tag{2.33}$$

and

$$\eta(\phi) \equiv m_{\rm Pl}^2\frac{V''}{V} \ll 1, \tag{2.34}$$

which describe the slope and the curvature of the potential, respectively.

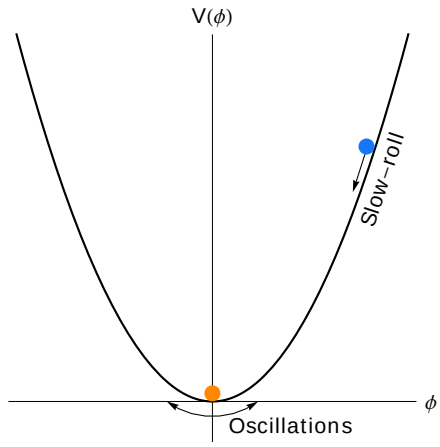

Figure 2.1: Illustration of the dynamics of the inflaton field in a quadratic potential, $V(\phi) = \frac{1}{2}m_\phi^2\phi^2$. During inflation the field slowly rolls down along the potential function which leads to the expansion of the space. After it reaches the minimum of the potential it begins to oscillate rapidly around the origin leading to a period of reheating which will be discussed in Sec. 2.6.

The end of inflation is taken as the moment when the second condition is no longer satisfied. An illustration of a simple quadratic potential function is given in Fig. 2.1.

2.5 Origin of the perturbations

As was explained in Section 2.4 the historical motivation for the period of inflation was in solving the problems plaguing standard cosmology. It was, however, rather soon understood that it can also explain the origin of the cosmic perturbations [17–19]. To see how these fluctuations are generated in the early Universe we have to quantize a scalar field in a de Sitter space and study its evolution with time.

To reach the quantum theory the field needs to be promoted to an operator and expanded in terms of the Fourier modes [32, 33]. The mode functions will then satisfy the same equation of motion as the classical fields. We will therefore solve the classical evolution of the field first and only then study the quantum behavior.

The evolution of the scale factor in a de Sitter space was given in Eq.

(2.17)

$$a(\eta) = -\frac{1}{H\eta}, \tag{2.35}$$

where the conformal time, η, goes from $-\infty$ to 0 and the Hubble parameter, H, is a constant. We will assume that the scalar field ϕ (not necessarily the inflaton) is massive with potential $V = \frac{1}{2}m_\phi^2\phi^2$ and that it is effectively light during inflation, *i.e.* $m_\phi \ll H$. By using a scaled field $u = a\phi$ in the action (2.25) and calculating the Euler-Lagrange equations, we get

$$u'' - \nabla^2 u + \Big(a(\eta)^2 m_\phi^2 - \frac{a''}{a}\Big)u = 0. \tag{2.36}$$

Expanding u in terms of the Fourier modes

$$u(\eta, \vec{x}) = \int \frac{d^3k}{(2\pi)^{3/2}} u_k(\eta) e^{i\vec{k}\cdot\vec{x}} \tag{2.37}$$

we obtain the equations of motion for the modes $u_k(\eta)$

$$u_k'' + \omega_k^2(\eta) u_k = 0, \tag{2.38}$$

where

$$\omega_k^2(\eta) = k^2 + a(\eta)^2 m_\phi^2 - \frac{a''}{a} = k^2 + \Big(\frac{m_\phi^2}{H^2} - 2\Big)\frac{1}{\eta^2}. \tag{2.39}$$

By setting $k\eta = -s$ and $u_k = \sqrt{s} f$, we can write this equation as

$$s^2 \frac{d^2 f}{ds^2} + s\frac{df}{ds} + \Big(s^2 - \Big(\frac{9}{4} - \frac{m_\phi^2}{H^2}\Big)\Big) f = 0 \tag{2.40}$$

which is the Bessel equation. The solution of the mode function then reads

$$u_k(\eta) = \sqrt{-k\eta}\Big(AJ_n(-k\eta) + BY_n(-k\eta)\Big), \tag{2.41}$$

where J_n and Y_n are Bessel functions of first and second kind, respectively, A and B are some constants of integration (that can depend on k) and $n = \sqrt{\frac{9}{4} - \frac{m_\phi^2}{H^2}}$. It is customary to write the solution in terms of the Hankel functions [34] which in general leads to a shorter notation. We will, however, follow Ref. [33] which uses Bessel functions of the first and the second kind.

The solution now essentially depends on the magnitude of $|\eta|/(1/k)$, *i.e.* the ratio of the comoving particle horizon to the comoving wavelength of the perturbations. In de Sitter space this is initially very large ($\eta \to -\infty$)

and asymptotically approaches value 0 at late times. To get the solutions of these two cases, it is sufficient [33] to concentrate on the approximate forms of the mode equation (2.38). At early times we can neglect η^{-2} terms, $\omega_k^2 \to k^2$ and we select

$$u_k(\eta) \propto e^{ik\eta} \tag{2.42}$$

as the solution. At late times $\eta^{-2} \gg k^2$ and we can neglect the momentum term. The equation of motion then reads

$$u_k'' - \left(2 - \frac{m_\phi^2}{H^2}\right)\frac{1}{\eta^2}u_k = 0, \tag{2.43}$$

where we have assumed that $m_\phi \ll H$ during inflation. By a change of variable $-\eta = e^x$, we can transform Eq. (2.43) into a homogeneous second order differential equation with constant coefficients. The solution then reads

$$u_k(\eta) = A_1|\eta|^{\lambda_1} + A_2|\eta|^{\lambda_2}, \tag{2.44}$$

where

$$\lambda_{1,2} = \frac{1}{2} \pm \sqrt{\frac{9}{4} - \frac{m_\phi^2}{H^2}}. \tag{2.45}$$

The dominant term is the latter with smaller exponent. For $m_\phi \ll H$ we can approximate $\lambda_2 \approx -1$ and

$$u_k(\eta) \approx A_2|\eta|^{-1}. \tag{2.46}$$

Physically these different solutions tell that the original field $\phi_k = u_k/a$ evolves initially like $1/a$ during the inflation. However, once the modes are driven larger than the Hubble horizon ($k|\eta| = 1$) they plateau to a constant value. Note that for a heavy field, $m_\phi \gg H$, the square root term in Eq. (2.45) leads to an oscillating part and the amplitude of the modes evolves as $u_k(\eta) \propto |\eta|^{-1/2}$. In terms of the original field this means that the modes are diluted once they become larger than the Hubble horizon.

We will now promote the scaled field into an operator, $\hat{u}(\eta, \vec{x})$, and define the canonical momentum as $\hat{\pi}(\eta, \vec{x}) = d\hat{u}(\eta, \vec{x})/d\eta$. The equal-time commutation relations are postulated as

$$\begin{aligned} &[\hat{u}(\eta, \vec{x}), \hat{u}(\eta, \vec{y})] = [\hat{\pi}(\eta, \vec{x}), \hat{\pi}(\eta, \vec{y})] = 0, \\ &[\hat{u}(\eta, \vec{x}), \hat{\pi}(\eta, \vec{y})] = i\delta(\vec{x} - \vec{y}), \end{aligned} \tag{2.47}$$

where $[,]$ is the commutator and $\delta(\vec{x})$ the Dirac delta function. The mode

expansion then reads

$$\hat{u}(\eta,\vec{x}) = \frac{1}{(2\pi)^{3/2}}\int d^3k\Big(u_k^*(\eta)\hat{a}_{\vec{k}}e^{i\vec{k}\cdot\vec{x}} + u_k(\eta)\hat{a}_{\vec{k}}^\dagger e^{-i\vec{k}\cdot\vec{x}}\Big), \tag{2.48}$$

where $\hat{a}_{\vec{k}}$ and $\hat{a}_{\vec{k}}^\dagger$ are the annihilation and creation operators, respectively, and k is the comoving momentum. From commutators (2.47) and the mode expansion it now follows [32, 33] that

$$\begin{aligned}\left[\hat{a}_{\vec{k}},\hat{a}_{\vec{k}'}\right] &= \left[\hat{a}_{\vec{k}}^\dagger,\hat{a}_{\vec{k}'}^\dagger\right] = 0,\\ \left[\hat{a}_{\vec{k}},\hat{a}_{\vec{k}'}^\dagger\right] &= \delta(\vec{k}-\vec{k}'),\end{aligned} \tag{2.49}$$

on the condition that the mode functions are normalized as

$$u_k^*(\eta)u_k'(\eta) - u_k^{*\prime}(\eta)u_k(\eta) = i. \tag{2.50}$$

The solution of the mode function Eq. (2.41), however, has two constants of integration meaning that even after satisfying the normalization condition there still remains some freedom. In terms of the quantum theory this means the definition of the vacuum is not unique in a de Sitter space. This also implies that by defining a vacuum at some time η_0 it generally is no longer empty at some later time η_1, which can be interpreted as the production of scalar particles during inflation [32, 33].

A solution to this ambiguity is to use a Bunch-Davies vacuum that at early times matches the Minkoswki vacuum [33, 34]. This can be seen as a rather natural choice since at early times the observationally interesting modes are assumed to be inside the horizon and the influence of gravity can be neglected. In terms of the mode functions this means that at early times we have

$$u_k(\eta) = \frac{1}{\sqrt{2k}}e^{ik\eta}. \tag{2.51}$$

By demanding that the full solution (2.41) approaches this at the early time limit, we obtain

$$u_k(\eta) = \frac{\sqrt{-\pi\eta}}{2}C\Big(J_n(-k\eta) - iY_n(-k\eta)\Big), \tag{2.52}$$

where $C = \exp\Big(i(n\pi/2 - \pi/4)\Big)$.

The variance of the original scalar field, $\hat{\phi} = \hat{u}/a$, can be now calculated

in the momentum space as

$$\begin{aligned}\langle 0|\hat{\phi}^{\dagger}_{\vec{k}}\hat{\phi}_{\vec{k}'}|0\rangle &= \frac{1}{a^2}\langle 0|\hat{u}^{\dagger}_{\vec{k}}\hat{u}_{\vec{k}'}|0\rangle = \frac{1}{a^2}u_k(\eta)u_k^*(\eta)\langle 0|\hat{a}^{\dagger}_{\vec{k}}\hat{a}_{\vec{k}'}|0\rangle \\ &= (H\eta)^2 u_k(\eta)u_k^*(\eta)\delta(\vec{k}-\vec{k}').\end{aligned} \tag{2.53}$$

At small values of $-k\eta$, Bessel function of the second kind dominates and we can write

$$u_k(\eta)u_k^*(\eta) \to \frac{1}{2k^3\eta^2} \tag{2.54}$$

from the asymptotic form of Y_n for massless field with $n = 3/2$ [35]. The variance of the scalar field then reads at late times

$$\langle 0|\hat{\phi}^{\dagger}_{\vec{k}}\hat{\phi}_{\vec{k}'}|0\rangle = \delta(\vec{k}-\vec{k}')\frac{H^2}{2k^3}. \tag{2.55}$$

It is customary to define the power spectrum, $\mathcal{P}_g$, of a generic field $g(\eta, x)$ as [36]

$$\langle 0|\hat{g}^{\dagger}_{\vec{k}}\hat{g}_{\vec{k}'}|0\rangle = \delta(\vec{k}-\vec{k}')\frac{2\pi^2}{k^3}\mathcal{P}_g. \tag{2.56}$$

The variance of the field $g(\eta, x)$ then reads in the position space

$$\begin{aligned}\langle 0|g^2(\eta,x)|0\rangle &= \int \frac{d^3k}{(2\pi)^{3/2}}\int \frac{d^3k'}{(2\pi)^{3/2}}e^{-i(\vec{k}-\vec{k}')\cdot\vec{x}}\langle 0|\hat{g}^{\dagger}_{\vec{k}}\hat{g}_{\vec{k}'}|0\rangle \\ &= \int \mathcal{P}_g(k)\, d(\ln(k))\end{aligned} \tag{2.57}$$

and the spectrum hence measures the contribution to the variance per unit logarithmic interval of k. From Eq. (2.55) we obtain the spectrum of the scalar field ϕ at late times

$$\mathcal{P}_{\phi} = \frac{H^2}{(2\pi)^2} \tag{2.58}$$

which means that the spectrum of super-horizon fluctuations is scale invariant in a de Sitter universe. Note that in this derivation we have assumed that H is a constant. During slow-roll inflation it will, however, also vary slightly which will make the spectrum (weakly) scale dependent [36].

2.6 Reheating the Universe

Reheating is an important part of early Universe cosmology (for a review cf. [30, 37]). After the inflation has terminated the Universe will be devoid of matter and all the energy will be stored in the scalar field(s) responsible for the inflaton. To restore the conditions of the Big Bang era, *i.e.* a Universe filled with radiation, a period of reheating is needed. This is usually achieved by coupling the scalar field directly to Standard Model matter sector into which the inflaton particles are assumed to decay. After all the energy has been drained from the scalar fields, the reheating process ends as soon as the decay products have reached thermal equilibrium. The temperature of the radiation at this point is called the reheat temperature.

2.6.1 Perturbative reheating

We will model the decay of scalar field first perturbatively. To this end, we start with the scalar field that has rolled slowly down the potential function and reached its minimum. It will then start to oscillate coherently around the minimum while losing energy and producing particles through some decay channel with decay width Γ. To take this into account we modify the field equation (2.26) to include a dissipative term $-\Gamma\dot{\phi}$ on the right hand side. By multiplying this with $\dot{\phi}$ and by averaging over a single period of an oscillation, it can be cast in the form of the continuity equation [30, 37]

$$\dot{\rho_\phi} + 3H\rho_\phi + \Gamma\rho_\phi = 0. \tag{2.59}$$

The decay products are often assumed to be light relativistic particles that slowly start to dominate the Universe. We therefore add an opposite term to the continuity equation of the decay products ψ,

$$\dot{\rho_\psi} + 3H(1+\omega_\psi)\rho_\psi - \Gamma\rho_\phi = 0, \tag{2.60}$$

where we have not set the equation of state of the decay products. By using the first Friedmann equation $H^2 = (\rho_\gamma + \rho_\phi)/(3m_{\rm Pl})$, we get a set of differential equations for the evolution of the system that can be solved. Initially $\rho_\psi = 0$ and $H > \Gamma$ in equation (2.59) and hence the decay process starts very slowly. Only when $H \sim \Gamma$ does particle production become effective and most of the energy is drained from the field. We can estimate the reheat temperature by setting $H \simeq \Gamma$ and the energy density equal to $\rho_\gamma \propto T^4$ (*i.e.* that of relativistic particles) in the first Friedmann equation.

The reheat temperature is then

$$T_{\rm RH} \simeq \sqrt{m_{\rm Pl}\Gamma} \tag{2.61}$$

which gives an estimate of the initial temperature of the hot Big Bang.

It is possible that the inflaton field might decay in addition into massive non-relativistic particles. Depending on the mass of these particles and the decay width, this might, however, cause the Universe to become matter dominated before the moment of nucleosynthesis at $T \sim 1$ MeV and spoil the thermal history of standard cosmology.

2.6.2 Preheating

The reheating period might also occur non-perturbatively through a violent preheating process [37, 38]. We will here concentrate mainly on the parametric resonance case as this is more relevant to this thesis than other possibilities such as instant [39] and tachyonic [40] preheating scenarios.

We will start with the homogeneous scalar field that has started the coherent oscillations around the minimum. We will concentrate on the massive inflaton with $V_\phi = \frac{1}{2}m_\phi^2\phi^2$ which we assume to be coupled to another bosonic field, χ. A fairly common choice is to take this to be mediated by a four-legged interaction Lagrangian

$$\mathcal{L}_{\rm int} = -\frac{1}{2}g^2\chi^2\phi^2. \tag{2.62}$$

We assume that χ is initially in a vacuum state. The inflaton will be treated as a classical field which is valid assuming that the amplitudes of the Fourier modes satisfy $\phi_k\dot{\phi}_k \gg 1$ [41]. The evolution of χ needs to be then solved in the classical background of the oscillating inflaton field. We will first write the quantum field $\hat{\chi}$ in terms of the annihilation and creation operators $\hat{a}_k$ and $\hat{a}_k^\dagger$ similar to Eq. (2.48) as

$$\hat{\chi}(t,\vec{x}) = \frac{1}{(2\pi)^{3/2}}\int d^3k\Big(\chi_k^*(t)\hat{a}_k e^{i\vec{k}\cdot\vec{x}} + \chi_k(t)\hat{a}_k^\dagger e^{-i\vec{k}\cdot\vec{x}}\Big), \tag{2.63}$$

where k is the (comoving) momentum vector. The equation of motion of the mode functions, $\chi_k(t)$, then reads from Eq. (2.26)

$$\ddot{\chi}_k(t) + 3H\dot{\chi}_k(t) + \left(\frac{k^2}{a^2} + g^2\Phi(t)^2\sin^2(m_\phi t)\right)\chi_k(t) = 0, \tag{2.64}$$

where we have written

$$\phi(t) \approx \Phi(t) \sin(m_\phi t) \tag{2.65}$$

for the oscillating inflaton field and assumed that m_χ can be neglected. In a matter dominated space ($a(t) \propto t^{2/3}$) we can write $\ddot{\phi}(t) = t\,\phi(t)$ for which we have

$$\ddot{\phi}(t) + 3H\dot{\phi}(t) = t^{-1}\,\ddot{\tilde{\phi}}(t), \tag{2.66}$$

leading to an equation for a simple harmonic oscillator. The amplitude of the oscillations of $\phi(t)$ will hence decrease with time as $\Phi(t) \propto (m_\phi t)^{-1}$.

To solve equation (2.64) it is customary to first understand the evolution in the Minkowski space and then describe the differences caused by the expansion. We can therefore set $a = 1$, neglect the Hubble term in Eq. (2.64) and assume that the amplitude, $\Phi(t)$, is a constant. By defining $\tau = m_\phi t$, the Fourier mode equation can be then written in the form of Mathieu's differential equation

$$\frac{d^2\chi_k(t)}{d\tau^2} + \Big(A - 2q\cos 2\tau\Big)\chi_k(t) = 0, \tag{2.67}$$

where

$$A = 2q + \frac{k^2}{m_\phi^2} \quad \text{and} \quad q = \frac{g^2\Phi^2}{4m_\phi^2}. \tag{2.68}$$

According to the Floquet's theorem [42] the solutions of the Matthieu equation exhibit instabilities at certain k values and lead to exponential growth of the mode functions (and the production of χ particles). More formally we write

$$\chi_k \propto \exp(\mu_k \tau), \tag{2.69}$$

where μ_k is the Floquet exponent. The stability of the solutions has been presented in Figure (2.2) in terms of the Floquet exponent as a function of A and q, where the exponentially unstable regions have been colored to distinguish them from the stable white regions. Because of the form of A in Eq. (2.68) the relevant values are now above $A = 2q$ line in Figure (2.2).

The magnitude of q now determines how efficient the parametric resonance is. For $q \ll 1$ the resonance happens in very narrow bands at $A_k \simeq l^2$, $l = 1, 2, ...$ of which the most import one is the first with $k \simeq m_\phi$ (See Fig. (2.2).) In the opposing case $q \gg 1$ the resonance occurs in broad bands which in general lead to much more efficient particle production [37, 43]. The values of momenta at which the particles are created can be determined with the Wentzel-Kramers-Brillouin (WKB) approximation [37, 43]

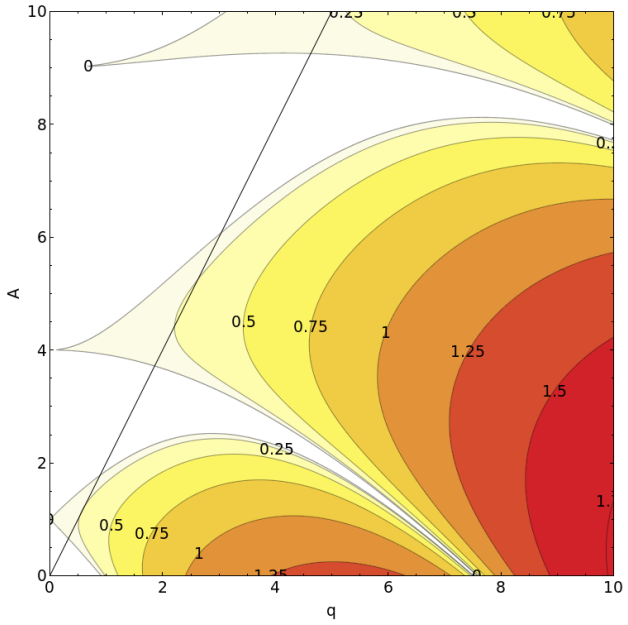

Figure 2.2: Stability map of the Mathieu equation as a function of A and q. In the white region the real part of the Floquet exponent is negative and the solutions are stable whereas the colored regions leads to exponential instability. The black line indicates the lower limit, $A = 2q$, of the physically relevant values. Different contours give the value of the Floquet exponent in the region. Note that the resonance bands extend all the way to $q = 0$ as very narrow stripes (not visible in the figure).

in which we write

$$\chi_k(t) \propto e^{\pm i \int \omega_k dt}, \tag{2.70}$$

where

$$\omega_k^2 = \frac{k^2}{a^2} + g^2 \Phi(t)^2 \sin^2(m_\phi t). \tag{2.71}$$

This approximation is valid as long as the effective frequency ω_k changes adiabatically, *i.e.* we have

$$\frac{d\omega_k}{dt} \lesssim \omega_k^2. \tag{2.72}$$

By solving where the effective mass of the χ_k modes changes non-adiabatically, we can determine the momenta values where particles are produced. For small values of ϕ we can approximate $\dot{\phi} \simeq m_\phi \Phi$ and insert ω_k from Eq.

(2.71) into the equality. The momentum values that violate the adiabaticity condition then satisfy

$$k^2 \lesssim (g^2 \phi m_\phi \Phi)^{2/3} - g^2 \phi^2. \tag{2.73}$$

Taking the right hand side as a function of ϕ gives the maximum band width when $\phi(t) = \phi_* = 3^{-3/4}\sqrt{m\Phi/g} \approx 1/2\sqrt{m\Phi/g}$. The particle production can be then understood to happen as bursts as the inflaton field oscillates around the origin.

The resonance in the expanding space can be understood similarly by studying the non-adiabaticity condition, *i.e.* Eq. (2.72). In this case it is however useful to instead take a scaled field $X_k(t) = a^{3/2}\chi_k(t)$ and apply the WKB approximation (2.70) to it. The new field evolves adiabatically most of the time (except for instances when it passes the origin) which leads to the exponential production of particles [43]. More quantitatively this process could be analyzed in terms of wave scatterings in a parabolic potential. We, however, omit these calculations and only cite the relevant results [37, 43].

The values of momenta where the particle production occurs are given by [43]

$$k^2/a^2 \lesssim \frac{g m_\phi \Phi}{\pi}. \tag{2.74}$$

The obvious implication is that as time progresses more comoving momenta k will satisfy this condition and will hence lead to a more effective preheating process. Another, less obvious, change is caused by the time evolution of the inflaton amplitude $\Phi(t)$. In Minkowski space the phase of a mode function χ_k is at a constant value when the inflaton passes the origin [37, 43]. In the expanding space the amplitude of the inflaton decreases with time which breaks this correlation between the phases of the mode functions and $\phi(t)$. This means the number density of χ particles can either increase or decrease depending on the value of this phase. However, roughly 75% of time the number density will still grow [37, 43]. Because of this behavior, that reminds of a random walk, broad resonance in an expanding space is frequently called stochastic resonance. The comoving number density of χ particles can be estimated with the wave scattering method as [43]

$$n_\chi(t) \sim \frac{k_*^3}{64\pi^2 a^3 \sqrt{\mu m_\phi t}} e^{2 m_\phi \mu t}, \tag{2.75}$$

where μ is an effective growth index of the resonance process and $k_* =$

$\sqrt{g m_\phi \Phi}$.

The preheating period ends when the back-reaction of the χ field becomes relevant, meaning that the interaction term $\frac{1}{2}g^2\chi^2\phi^2$ is of the same order of magnitude as $\frac{1}{2}m_\phi^2\phi^2$. The effective mass of the inflaton then starts to oscillate with the χ field leading eventually to the production of ϕ particles. The moment the preheating ends happens roughly when the number density of χ particles equals $n_\chi(t_{\rm br}) \sim m_\phi^2\Phi/g$ [43] which results in an implicit equation for the back-reaction time $t_{\rm br}$. Up to logarithmic corrections this can be estimated to be of order $t_{\rm br} \sim (\mu m_\phi)^{-1}$. During preheating $H \ll m_\phi$ and the length of the preheating period is hence generally much shorter than the Hubble time.

After the preheating comes to an end, different re-scattering processes start to dominate the evolution and the interactions between the fields become important. This part is difficult to describe analytically [37, 43] and numerical methods have to be used. To this end the scalar fields will be treated as classical waves, which is a valid assumption if the occupation numbers are high. The evolution of the system will be then solved in a discrete 3-dimensional lattice. These numerical methods will be discussed more closely in Chapter 4.

During the re-scattering period, fields that were not excited in the preheating stage also generate quanta at different k values. Through the interaction term (2.62) inflaton particles are created in annihilation process $\delta\chi_k\delta\chi_k \to \delta\phi_k\delta\phi_k$. Re-scattering where quanta $\delta\chi_k$ interact with the homogeneous inflaton mode, ϕ_0, also produces χ and ϕ particles. After this non-linear stage is over, the system enters a regime of turbulent dynamics during which the spectra of the field become smoother and start to evolve towards the UV part. The system is still, however, far from thermal equilibrium which is reached only after a time period much longer than the duration of the preheating and resonances processes.

After the preheating and re-scattering periods are over, much of the energy will be still stored in the inflaton field due the pairwise interactions of the Lagrangian (2.62) although these quickly cease as the space expands. These left-over inflaton particles could be considered to survive up to this day and act as a dark-matter component, although this is challenging to achieve without spoiling standard cosmology [44, 45]. It is usually assumed that the inflaton has additional couplings to other fields (for instance a Yukawa coupling to a fermion field) that complete the decay process [46].

Chapter 3

Cosmological perturbations

In the previous chapter we dealt with the unperturbed Universe and the birth of quantum fluctuations during a period of cosmic inflation. Next we will concentrate more closely on these small perturbations and their evolution. It is widely believed that these were the seeds from which the current structures within the Universe, *i.e.* stars, galaxies and galaxy clusters, grew over time through gravitational attraction. We will mostly concentrate on the linear perturbation theory although we will also present the results at the second order which we use in this thesis to calculate the level of non-Gaussianity generated in one curvaton model.

3.1 Cosmological perturbation theory

Cosmological perturbation theory was developed initially by Lifshitz in the 1940's [47]. It was, however, Bardeen [48] who first understood to concentrate on terms that are gauge independent and are easier to interpret physically. A review of cosmological perturbation theory can be found for example in Refs. [32, 36] which we follow closely.

3.1.1 Metric perturbations at first order

We will be working in conformal time to simplify the notation. The unperturbed line element in a flat FRW Universe was given in Eq. (2.14) and it reads

$$ds^2 = {}^{(0)}g_{\mu\nu}dx^\mu dx^\nu = a(\eta)^2(d\eta^2 - dx^i dx^i), \tag{3.1}$$

where ${}^{(0)}g_{\mu\nu}$ denotes the homogeneous background part. We include perturbations to the metric by simply writing

$$g_{\mu\nu} = g^{(0)}_{\mu\nu} + \delta g_{\mu\nu}, \tag{3.2}$$

where $\delta g_{\mu\nu}$ is the perturbation part.

To simplify the analysis it is useful to split $\delta g_{\mu\nu}$ into scalar, vector and tensor terms, depending on how they change in spatial rotations at constant-time hypersurfaces [32, 36]. A significant benefit from this decomposition is that different types of perturbations evolve independently at the linear order [32, 36] and hence can be studied separately.

Scalar perturbations are the most relevant for the generation of cosmic instabilities and structures and we concentrate on them. We will therefore construct the metric perturbations $\delta g_{\mu\nu}$ of only scalar terms. To this end we will use Helmholtz decomposition [36] to write a generic vector as $u_i = v_{,i} + v_i$ where v is a curl-free scalar term ($v_{[i,j]} = 0$), ${}_{,i} \equiv \partial_i$ and v_i is a divergence free ($\partial_i v_i = 0$) pure vector part. A similar decomposition can be done to a second order traceless tensor [36]

$$\Pi_{ij} = \Pi^S_{ij} + \Pi^V_{ij} + \Pi^T_{ij}, \tag{3.3}$$

where $\Pi^S_{ij} = (\partial_i\partial_j - \frac{1}{3}\gamma_{ij}\nabla^2)\Pi$, $\Pi^V_{ij} = \partial_i\Pi_j + \partial_j\Pi_i$ and Π^T_{ij} are the scalar, vector and pure tensor parts, respectively. Note that γ_{ij} is the spatial metric tensor and $\partial_i\Pi_i = 0$ and $\partial_i\Pi^T_{ij} = 0$ in the equations [36].

With these decompositions we can write the metric perturbation in terms of scalar functions. The spatial component δg_{ij} can be formed from a scalar by either multiplying with the spatial metric tensor γ_{ij} or by using the previous tensor decomposition. In a flat space $\gamma_{ij} = \delta_{ij}$ and covariant derivatives simplify to ordinary spatial derivatives. δg_{0j} and δg_{j0} transform like vectors and are hence equal to the gradient of a scalar due to the Helmholtz decomposition. Lastly, the time time component is already a scalar and hence the metric perturbation reads

$$\delta g_{\mu\nu} = a(\eta)^2 \begin{pmatrix} 2\phi & -B_{,i} \\ -B_{,i} & 2(\psi\delta_{ij} - E_{,ij}) \end{pmatrix} \tag{3.4}$$

or in terms of the line element

$$\begin{aligned} ds^2 = a(\eta)^2 \big\{ &(1+2\phi)d\eta^2 - 2B_{,i}d\eta dx^i \\ &-[(1-2\psi)\delta_{ij} + 2E_{,ij}]dx^i dx^j \big\}, \end{aligned} \tag{3.5}$$

where $B_{,i} = \frac{\partial B}{\partial x^i}$, $E_{,ij} = \frac{\partial^2 E}{\partial x^i \partial x^j}$ and we have embedded the Laplacian of the scalar E term in the ψ function. Note that $\delta g_{\mu\nu}$ has 10 components since it is a symmetric tensor. In the scalar-vector-tensor decomposition we are using these are divided among the different terms as 4, 4 and 2, respectively. In the scalar part these are given by the four independent functions ϕ, ψ, B and E. Note that these depend explicitly on the spacetime coordinates x^μ *e.g.* $\phi = \phi(\eta, x^i)$. We use a shorter notation when this dependence is omitted.

Vector perturbations are not generated by inflation and they can usually be neglected [32, 36, 49]. Tensor perturbations are responsible for the production of gravitational waves that can be useful when different models of inflation are compared [32, 36, 49]. We will not, however, study them in this thesis. Also note that the decomposition we have used is valid only for the linear first order terms. At higher order different perturbations are coupled to each other which means that for example vector and tensor perturbations are seeded by first order scalar terms [50].

3.1.2 Gauge transformations

In general relativity a choice of coordinate system is called a gauge. A gauge transformation then naturally means a change of the coordinate system. In this thesis we will concentrate only on infinitesimal coordinate transformations which we write as

$$\tilde{x}^\mu = x^\mu + \xi^\mu(x^\mu), \tag{3.6}$$

where $\xi^\mu(x^\mu) = (\xi^0(x^\mu), \gamma^{ij}\xi(x^\mu)_{,i} + \xi^i_{\rm V}(x^\mu))$ are small gauge parameters and we have decomposed the three vector $\xi^i(x^\mu)$ into a scalar $\gamma^{ij}\xi(x^\mu)_{,i}$ and a pure vector part $\xi^i_{\rm V}(x^\mu)$ for which $\partial_i \xi^i_{\rm V}(x^\mu) = 0$. Since we are now interested only in the scalar terms we will set $\xi^i_{\rm V} = 0$ and Eq. (3.6) then reads

$$\eta \to \eta + \xi^0, \;\; x^i \to x^i + \gamma^{ij}\xi_{,j}. \tag{3.7}$$

The metric tensor (component) $g_{\mu\nu}(x)$ now changes in a coordinate transformation $x^\mu \to \tilde{x}^\mu$ as

$$\tilde{g}_{\mu\nu}(\tilde{x}) = g_{\alpha\beta}(x)\frac{\partial x^\alpha}{\partial \tilde{x}^\mu}\frac{\partial x^\beta}{\partial \tilde{x}^\nu}. \tag{3.8}$$

By applying this rule to the full perturbed metric tensor $g_{\mu\nu}$, inserting in Eq. (3.7), expanding $g_{\mu\nu}(x)$ as a series and by finally re-ordering the terms

we get the transformation rules of the scalar perturbations

$$\begin{aligned}\tilde{\phi} &= \phi - \frac{a'}{a}\xi^0 - \xi^{0\prime} \\ \tilde{B} &= B + \xi^0 - \xi' \\ \tilde{\psi} &= \psi + \frac{a'}{a}\xi^0 \\ \tilde{E} &= E - \xi.\end{aligned} \tag{3.9}$$

As is evident from these equations the values of the scalar perturbations depend on the choice of gauge. A simple remedy is to fix the coordinate transformation parameters ξ^0 and ξ *i.e.* the used gauge and to study if the perturbations are physical in the sense that they are free of any residual gauge freedoms. It is customary to instead define the gauge in terms of the scalar perturbation variables of which two can be fixed. Historically the synchronous gauge with conditions $\phi = 0$ and $B = 0$ and the Newtonian (or the longitudinal) gauge with $E = 0$ and $B = 0$ are frequently used. Note, however, that even after fixing the gauge some coordinate transformations are still allowed in the synchronous gauge leading to some physicality related difficulties [32]. Nowadays these problems are well understood and the synchronous gauge is frequently used in computational cosmology, *e.g.* in the CMBFAST code [51]. The longitudinal gauge does not suffer from harmful spurious gauge modes, which makes its use appealing.

Another cure for the gauge dependence is to search for variables that are independent of the gauge. From the linear scalar metric perturbations we can construct variables

$$\Phi_L = \phi + \frac{1}{a}[(B - E')a]', \ \Psi_L = \psi - \frac{a'}{a}(B - E') \tag{3.10}$$

that are independent under gauge transformations (3.9). These were first presented by Bardeen [48] and are hence called the Bardeen potentials.

3.1.3 Perturbations of the stress-energy tensor

Up to this point we have been dealing with the metric perturbations. To understand the generation of cosmic structures we also have to include perturbations in the stress-energy tensor on the right hand side of the Einstein equation (2.3). We will assume that it is of the perfect-fluid type (Eq. (2.4))

meaning that the unperturbed stress-energy tensor reads

$$^{(0)}T^{\nu}_{\mu} = (\rho + p)u_{\mu}u^{\nu} - p\delta^{\nu}_{\mu}. \tag{3.11}$$

Scalar perturbations are described with four independent functions [32]: the energy density and pressure perturbations $\delta\rho$ and δp, respectively, velocity potential v and the anisotropic stress term σ. We will assume that the last term can be neglected and hence the perturbed energy tensor tensor reads [32]

$$\begin{aligned} \delta T^0_0 &= \delta\rho \\ \delta T^0_i &= (\rho + p)a^{-1}v_{,i} \\ \delta T^i_j &= -\delta p\delta^i_j. \end{aligned} \tag{3.12}$$

To determine how the energy and pressure density change under gauge transformations it is instructive to consider a generic time dependent function, $f(\eta)$, under the time change $\eta \to \eta + \xi^0$. Now the value of the perturbed function does not change and hence

$$f(\eta) + \delta f(\eta, \vec{x}) = f(\tilde{\eta}) + \widetilde{\delta f}(\eta, \vec{x}), \tag{3.13}$$

from which it follows that to first order

$$\widetilde{\delta f}(\eta, \vec{x}) - \delta f(\eta, \vec{x}) = f(\eta) - f(\tilde{\eta}) \approx -f'\xi^0. \tag{3.14}$$

In the corresponding spatial transformations the perturbed function, δf, does not change since the background value is independent of the position. We can now use Eq. (3.14) to deduce the transformation rules

$$\begin{aligned} \widetilde{\delta\rho} &= \delta\rho - \rho'\xi^0, \\ \widetilde{\delta p} &= \delta p - p'\xi^0. \end{aligned} \tag{3.15}$$

For the velocity term v the gauge transformation reads

$$\tilde{v} = v - a\xi^0. \tag{3.16}$$

It is now possible to define a coordinate transformation in terms of these stress-energy tensor perturbations also. The so called uniform density gauge [36] is often used gauge, for which $\widetilde{\delta\rho} = 0$ meaning that $\xi^0 = \delta\rho/\rho'$. The curvature perturbation is defined as the ψ term of the metric tensor

perturbations. Its value in the uniform density gauge reads

$$-\zeta \equiv \psi + \frac{\mathcal{H}}{\rho'}\delta\rho, \tag{3.17}$$

which is an often studied quantity in cosmology. Notably it is gauge invariant by construction. Note too that if the pressure perturbation is adiabatic, *i.e.* $\delta p = c_{\rm s}^2\delta\rho$, where $c_{\rm s}^2 = P'/\rho'$ is the adiabatic sound speed, ζ is a constant on scales larger than the Hubble length [36].

Similarly the curvature perturbation can be defined [36] on the hypersurface of uniform density gauge of a single fluid component (*i.e.* with $\delta\rho_\alpha = 0$) as

$$-\zeta_\alpha \equiv \psi + \frac{\mathcal{H}}{\rho'_\alpha}\delta\rho_\alpha. \tag{3.18}$$

This is related to the total curvature perturbation ζ as

$$\zeta = \sum_i \frac{\rho'_i}{\rho'}\zeta_i, \tag{3.19}$$

where $\rho' = \sum_i \rho'_i$. Note that if the continuity equations ρ'_i include dissipating terms Q_i which is often the case during reheating the curvature perturbation terms become ill-defined when $\rho'_i = 0$. This does not mean that the perturbation theory is invalid. It only signals that the gauge is ill-defined and one remedy is to solve the evolution in another gauge where these problems are avoided. In this case one choice is to use the uniform curvature (or flat) gauge with $\tilde{\psi} = 0$ meaning that

$$\zeta = -\frac{\mathcal{H}}{\rho'}\delta\rho. \tag{3.20}$$

Another possibility is to solve the evolution of the energy perturbation $\delta\rho$ in the flat gauge in which case we use

$$\widetilde{\delta\rho} \equiv \delta\rho + \frac{\rho'}{\mathcal{H}}\psi \tag{3.21}$$

as the variable. Note that we use this method in research articles [1–3] where we solve the evolution of ζ_α by first evolving the density perturbations in the flat gauge and then use formula (3.18) to calculate the curvature perturbation.

The curvature perturbation can also be calculated using a comoving slicing at which the velocity perturbation $\tilde{v}$ vanishes, meaning that $\xi^0 =$

$a^{-1}v$. The comoving curvature perturbation then reads

$$\mathcal{R} \equiv \psi + \mathcal{H}\frac{v}{a} \tag{3.22}$$

which is also gauge invariant by construction.

It can be shown [52] that the two different gauge invariant curvature perturbation variables are related by equality

$$-\zeta = \mathcal{R} + \frac{2\rho}{3(p+\rho)}\Big(\frac{k}{aH}\Big)^2 \Psi_L, \tag{3.23}$$

where Ψ_L is one of the Bardeen potentials. On large scales $k \to 0$ and hence the values of the two curvature perturbations coincide.

3.1.4 Evolution of the perturbations

Now that we have defined different scalar perturbations and presented how they change in gauge transformations the equations of motion of the perturbations need to be determined. We are interested mainly in the evolution of the curvature perturbation ζ and will therefore only present the relevant equations. We will also confine the evolution to length scales λ larger than the Hubble scale which means that in terms of the comoving wave number we have

$$\frac{k}{aH} \ll 1. \tag{3.24}$$

As a consequence the gradient terms can be neglected, making it much easier to determine the evolution of the system.

In the multi-fluid formalism that we are using the evolution of the metric perturbations is determined from the Einstein equations

$$G_{\mu\nu} = -8\pi G T_{\mu\nu} \tag{3.25}$$

whereas the evolution of the fluid perturbations is given by the covariant continuity equation

$$D_\mu T^{\mu\nu} = 0. \tag{3.26}$$

The calculation of these is straightforward but tedious. We will therefore only present the equations of motion. The full derivation of these equations can be found for example in Refs. [32, 36, 49, 53, 54].

We will assume that there are multiple interacting fluids for which

$$\rho_i' = -3\mathcal{H}(1+\omega_i)\rho_i + Q_i, \tag{3.27}$$

where Q_i is the interaction term with constraint $\sum_i Q_i = 0$. Perturbing the covariant continuity equations, one finds the evolution equations of the energy and pressure density perturbations, $\delta\rho_i$ and δP_i, respectively, on large scales [54]

$$\delta\rho_i' + 3\mathcal{H}(\delta\rho_i + \delta p_i) - 3(\rho_i + p_i)\psi' = a(Q_i\phi + \delta Q_i), \tag{3.28}$$

where δQ_i is the perturbed interaction term.

In addition, we have the G_0^0 component of perturbed Einstein equations [32, 53, 55]

$$3\mathcal{H}\big(\psi' + \mathcal{H}\phi\big) = -4\pi G a^2 \delta\rho, \tag{3.29}$$

where $\delta\rho = \sum_i \delta\rho_i$. For perfect fluids $\phi = \psi$ in the Newtonian gauge [32] and hence given the equations of state, ω_i, and the interactions between the fluids, Q_i, one can evolve the individual fluid perturbations along with the metric perturbation ϕ.

The evolution of the curvature perturbation ζ_i can be then derived from Eqs. (3.28) and (3.29) and it reads

$$\zeta_i' = \frac{3\mathcal{H}^2\delta P_{int(i)}}{\rho_i'} - \frac{\mathcal{H}}{\rho_i'}\delta Q_{int(i)} - (\mathcal{H}' - \mathcal{H}^2)\frac{Q_i}{\rho_i'}(\zeta - \zeta_i), \tag{3.30}$$

where $\delta P_{int(i)} \equiv \delta P_i - p_i'\delta\rho_i/\rho_i'$ and $\delta Q_{int(i)} \equiv \delta Q_i - Q_i'\delta\rho_i/\rho_i'$. Note that for non-interacting perfect fluids we have $\zeta_i' = 0$ and hence the curvature perturbations for each fluid remains constant in the long-wavelength limit.

3.1.5 Perturbations at second order

In some cases in cosmology, especially when calculating the non-Gaussianity of the CMB, higher order perturbation terms are needed [21]. We will therefore present the perturbation theory also at the second order. Essentially the description of the perturbations, gauge transformations and evolution equations is very similar to the first order. The major differences are the increase in the number of the needed perturbations and the coupling of the scalar, vector and tensor perturbations. The results presented in the previous sections remain valid, meaning that the vector and tensor perturbations can be neglected at first order.

We will follow closely to the notation of [21]. Note also that we will now use physical time t instead of the conformal time. The background is again assumed to be a spatially flat Friedmann-Robertson-Walker Universe. The metric tensor can be in this case expanded up to second order in the form

[21, 50, 56]

$$
\begin{aligned}
g_{\mu\nu}dx^\mu dx^\nu = &-(1+2\phi^{(1)}+\phi^{(2)})dt^2 + a(t)(\hat{\omega}_i^{(1)} + \frac{1}{2}\hat{\omega}_i^{(2)})dtdx^i \\
&+ a(t)^2\Big[(1-2\psi^{(1)}-\psi^{(2)})\delta_{ij} + \chi_{ij}^{(1)} + \frac{1}{2}\chi_{ij}^{(2)}\Big]dx^i dx^j,
\end{aligned}
\tag{3.31}
$$

where $a(t)$ is the scale factor and $\phi^{(r)}$, $\hat{\omega}_i^{(r)}$, $\psi^{(r)}$ and $\chi_{ij}^{(r)}$ are perturbation functions defined in [21] at first ($r = 1$) and second order ($r = 2$). When compared to the first order perturbed metric (3.5), B and E terms have been now replaced with $\hat{\omega}_i^{(r)}$ and $\chi_{ij}^{(r)}$ functions, respectively. It is customary to use a similar splitting to the first order theory to decompose the perturbations into scalar, vector and tensor terms. We can thus write [21]

$$
\hat{\omega}_i^{(r)} = \partial_i\omega^{(r)} + \omega_i^{(r)} \tag{3.32}
$$

and

$$
\chi_{ij}^{(r)} = \chi_{ij}^{(r)S} + \chi_{ij}^{(r)V} + \chi_{ij}^{(r)T}, \tag{3.33}
$$

where $\chi_{ij}^{(r)S} = (\partial_i\partial_j - \frac{1}{3}\gamma_{ij}\nabla^2)\chi^{(r)}$, $\chi_{ij}^{(r)V} = \partial_i\chi_j^{(r)} + \partial_j\chi_i^{(r)}$ and $\chi_{ij}^{(r)T}$ are the scalar, vector and pure tensor parts, respectively. The first order vector terms can be now neglected from these expressions as was also done previously in the linear theory [21].

At second order the different gauges can be also given in terms of the perturbation functions: for example the Poisson gauge is defined as $\omega^{(r)} = \chi^{(r)} = \chi_i^{(r)} = 0$ which is a generalized version of the longitudinal gauge that includes also higher order terms. For the spatially flat gauge we have $\psi^{(r)} = \chi^{(r)} = 0$ [21].

One finds the evolution equations of the density perturbations again from the covariant continuity equation. At first order the evolution equation is naturally the same as before, *i.e.* Eq. (3.28). At second order the equation reads (on large scales) [54]

$$
\begin{aligned}
&\dot{\delta\rho_i^{(2)}} + 3H(\delta\rho_i^{(2)} + \delta P_i^{(2)}) - 3(\rho_i + P_i)\dot{\psi}^{(2)} \\
&- 6\dot{\psi}^{(1)}[\delta\rho_i + \delta P_i + 2(\rho_i + P_i)\psi^{(1)}] \\
&= Q_i\phi^{(2)} + \delta Q_i^{(2)} - Q_i(\phi^{(1)})^2 + 2\phi^{(1)}\delta Q_i^{(1)}.
\end{aligned}
\tag{3.34}
$$

We also need the Einstein equations for the metric perturbations. In the Poisson gauge at first order we have $\psi^{(1)} = \phi^{(1)}$ and on large-scales $2\phi^{(1)} + 2\dot{\psi}^{(1)}/H = -\delta\rho/\rho_0$, whereas in the spatially flat gauge $\psi^{(1)} = \chi^{(1)} =$

0 and $2\phi^{(1)} = -\delta\rho/\rho_0$ [21]. At second order the equations get more complex and they are presented in detail in Ref. [21]. The equations which we will need are the $0-0$ and $i-j$-components of the Einstein equations on large scales which read in the Poisson gauge in a matter dominated universe

$$\begin{aligned}\phi^{(2)} =& -\frac{1}{2}\frac{\delta\rho^{(2)}}{\rho_0} + 4(\psi^{(1)})^2 \\ \psi^{(2)} - \phi^{(2)} =& -4(\psi^{(1)})^2 - \frac{10}{3}\nabla^{-2}(\partial^i\psi^{(1)}\partial_i\psi^{(1)}) \\ &+ 10\nabla^{-4}\Big(\partial^i\partial_j\Big(\partial_i\psi^{(1)}\partial^j\psi^{(1)}\Big)\Big),\end{aligned} \tag{3.35}$$

where ∇^{-2} is the inverse of the Laplacian. In the spatially flat gauge the $0-0$-component is

$$\phi^{(2)} = -\frac{1}{2}\frac{\delta\rho^{(2)}}{\rho_0} + 4(\phi^{(1)})^2. \tag{3.36}$$

The gauge invariant curvature perturbation can be also generalized to the second order. For fluid component i it reads

$$\begin{aligned}\zeta_i^{(2)} =& -\psi^{(2)} - \frac{\delta\rho_i^{(2)}}{\rho_i'} + 2\frac{\delta\rho_i^{(1)\prime}}{\rho_i'}\frac{\delta\rho_i^{(1)}}{\rho_i'} + 2\frac{\delta\rho_i^{(1)}}{\rho_i'}(\psi^{(1)\prime} + 2\psi^{(1)}) \\ &- \Big(\frac{\delta\rho_i^{(1)}}{\rho_i'}\Big)^2\Big(\frac{\rho_i''}{\rho_i'} - 2\Big).\end{aligned} \tag{3.37}$$

The definition of this curvature perturbation fails similarly to the first order case when $\rho_i' = 0$. Therefore in the numerical calculations we have used the spatially flat gauge which is not plagued by these issues. The corresponding equations of motion can be easily read from Eqs. (3.28) and (3.34) by going to the spatially flat gauge $\psi^{(r)} = \chi^{(r)} = 0$.

3.2 Spectrum of the curvature perturbation

To validate a cosmological model it is imperative to compare it to observations. The comparison of different scalar field models to the CMB radiation can be done with the curvature perturbation which is related to the observed temperature anisotropies through the Sachs-Wolfe effect $\Delta T/T = \zeta/5$ on large scales [30, 57]. Power spectrum of the CMB radiation anisotropies can be then used to give limits on the cosmological model.

3.2.1 Slow-roll inflation

The production of the curvature perturbation during slow-roll inflation is often studied with the comoving curvature perturbation $\mathcal{R}$. During inflation it follows from Eq. (2.28) that

$$p + \rho = \frac{\phi_0'^2}{a^2} \tag{3.38}$$

where ϕ_0 is the homogeneous inflaton field. The perturbed stress energy tensor reads [32]

$$\delta T_i^0 = a^{-2}\phi_0'\delta\phi_{,i}, \tag{3.39}$$

where $\delta\phi$ is the first order field perturbation. By comparing this to the perfect fluid case, *i.e.* Eq. (3.12), and using Eq. (3.38), the velocity perturbation can be solved as

$$\frac{v}{a} = \frac{\delta\phi}{\phi_0'}. \tag{3.40}$$

From the definition of the comoving curvature perturbation, Eq. (3.22), it then follows that

$$\mathcal{R} = \psi + \mathcal{H}\frac{\delta\phi}{\phi_0'} = \psi + H\frac{\delta\phi}{\dot{\phi}_0}. \tag{3.41}$$

In the spatially flat gauge the spectrum of the curvature perturbations then reads

$$\mathcal{P}_\mathcal{R} = \left(\frac{H}{\dot{\phi}_0}\right)^2 \mathcal{P}_{\delta\phi} = \left(\frac{H}{\dot{\phi}_0}\right)^2 \left(\frac{H}{2\pi}\right)^2 \tag{3.42}$$

where we have used the spectrum of light fields, *i.e.* Eq. (2.58), for the field perturbations. During slow-roll inflation the time derivative of the field can be solved in terms of the potential and the Hubble parameter from Eq. (2.32) as $3H\dot{\phi}_0 = -V'$. By using the definition of the $\epsilon(\phi)$ parameter from Eq. (2.33), the spectrum of the curvature perturbation can be written as

$$\mathcal{P}_\mathcal{R} = \frac{1}{24\pi^2 m_{\rm Pl}^4}\frac{V}{\epsilon(\phi)}. \tag{3.43}$$

The left hand side can be measured from the CMB radiation and used to set limits on the used inflation model.

3.2.2 Curvaton scenario

Up to this point we have been mostly dealing with the evolution of the inflaton field in the early Universe. The results of Sec. 2.5, however, hold for

any light field during inflation, meaning that they also acquire fluctuations with a scale free spectrum.

The curvaton mechanism [58–64] is a much studied alternative to the standard inflationary paradigm for the origin of the observed primordial perturbations. The curvaton field, σ, is assumed to be effectively light and subdominant during the inflation process and unable to drive the expansion of space. After this period is over the Universe will be radiation dominated and the curvaton field will start to oscillate coherently, approximately when $H \simeq m_\sigma$, where m_σ is the mass of the curvaton. In the simplest scenario with $V_\sigma = \frac{1}{2}m_\sigma^2\sigma^2$ the energy density of the curvaton will then evolve like non-relativistic matter ($\propto a^{-3}$) whereas the radiation evolves like $\propto a^{-4}$. As a result, the contribution of the curvaton density will grow with time and it can become the dominating element of the Universe.

The decay process is often modeled perturbatively similar to Sec. 2.6.1 by assuming that the curvaton is coupled to radiation or matter component. If the curvaton starts to dominate the energy content before the decay process becomes significant, *i.e.* when $H \simeq \Gamma_\sigma$, the moment of decay can be understood as a second reheating of the Universe.

One of the main motivations for the curvaton paradigm is to liberate the inflation model from the constraint to produce the observed amplitude of the CMB anisotropy spectrum. This can resolve fine tuning issues in different inflation models [20] while still leading to adiabatic perturbations consistent with the current observational data [24, 25].

The development of curvature perturbations in the curvaton scenario can be calculated starting from Eq. (3.19)

$$\zeta = \sum_i \frac{\rho_i'}{\rho'}\zeta_i. \tag{3.44}$$

We will assume that the Universe consists of two components: the curvaton field and the radiation (γ). The total curvature perturbation then reads

$$\zeta = (1-f)\zeta_\gamma + f\zeta_\sigma, \tag{3.45}$$

where

$$f = \frac{3\rho_\sigma}{4\rho_\gamma + 3\rho_\sigma} \tag{3.46}$$

and we have assumed that the decay rate Γ_σ can be neglected. In the

curvaton scenario we will assume that $\zeta_\gamma \approx 0$ and hence

$$\zeta \approx f\zeta_\sigma. \tag{3.47}$$

In the spatially flat gauge ($\psi = 0$) we can write

$$\zeta_\sigma = \frac{\delta\rho_\sigma}{3\rho_\sigma} \tag{3.48}$$

and for the quadratic potential $V_\sigma = \frac{1}{2}m_\sigma^2\sigma^2$ we can approximate

$$\frac{\delta\rho_\sigma}{\rho_\sigma} \simeq 2\frac{\delta\sigma}{\sigma}. \tag{3.49}$$

In this case the perturbation $\delta\sigma$ and the field have the same equation of motion and hence the ratio stays constant.

We will now assume that the curvaton field decays through the sudden decay approximation which means that once $H = \Gamma_\sigma$ the decay of the curvaton is immediate. This is a pragmatic assumption which makes the analytical calculations easy to perform. More accurate results could be determined numerically. The total curvature perturbation then reads

$$\zeta \approx \frac{2}{3}f_{\mathrm{dec}}\frac{\delta\sigma}{\sigma}\Big|_*, \tag{3.50}$$

where f_{dec} is the energy fraction calculated at the moment of decay and the asterisk, $*$, means that the field values are calculated at the time of inflation. The spectrum of the curvature perturbation then reads

$$\mathcal{P}_\zeta \approx \frac{f_{\mathrm{dec}}^2}{9\pi^2}\frac{H_*^2}{\sigma_*^2}. \tag{3.51}$$

Similar to the slow-roll inflation case, the left hand side can be determined from the CMB radiation and used to limit the studied model.

Chapter 4

Computational methods

In the previous chapter we presented the main features of the cosmological perturbation theory. If there is, however, a period of preheating before the usual reheating commences, we are compelled to use non-perturbative methods to understand the evolution of the Universe and its energy content. This is most often done by treating the scalar fields as classical objects which are evolved numerically in a discrete lattice. Publicly available programs that are designed to do this include LATTICEEASY [65], DEFROST [66], PSpectRe [67] and HLATTICE [68].

In this thesis a lot of effort has been put to develop and to improve the computational methods that are needed when studying the preheating of the Universe. As a result we were able to produce two publicly available programs called CUDAEASY and PyCOOL [4, 5] that were the first to use graphics processing units (GPUs) to accelerate the numerical computations in the realm of the very early Universe. The speed of the program is, however, secondary to the accuracy of the results. In the PyCOOL program we have in addition implemented a symplectic integrator that can preserve the form of the first Friedmann equation to high accuracy and therefore lead to very precise results. We will next present the salient features of these codes with the emphasis being on the PyCOOL program.

4.1 GPGPU computing

General-purpose computing on graphics processing units (GPGPU) is a rather new method where computationally difficult problems are accelerated with GPUs to get significantly shorter program run-times [69–89]. In general the problem is divided into small pieces that are then solved in

a massively parallel fashion. Usually this means that the number of the calculating threads is counted in the thousands.

The programs developed as a part of this thesis use NVIDIA's CUDA (an acronym for Compute Unified Device Architecture) to run codes on the GPUs. This was introduced in November 2006 as a programming language for NVIDIA GPUs [90, 91]. CUDA comes with C for CUDA application programming interface that gives programmers familiar with C an easy way to start writing programs that are executed on GPU. This is achieved by extending C with different CUDA commands.

Within the CUDA framework GPUs are called *devices* whereas the CPU is known as the *host*. The fundamental concept in GPGPU are the lightweight *threads* which are executed in parallel on the device with *kernel* functions. Threads within a kernel constitute a two dimensional *grid* that is divided into different *blocks* that hold the threads. Blocks can be one, two or three dimensional and threads within the same block can share information through a *shared memory*. Threads and blocks have IDs (threadIdx and blockIdx respectively) which can be used to calculate the global thread indexes within the grid.

The device has a range of memories with different characteristics and roles in computing. *Global* or *device memory* is the main memory of the GPU but it is located off-chip and therefore has a considerable latency. Reads from the global memory should be organized in certain way (*coalesced*) to achieve maximum bandwidth although in newer devices there are cache memories that can alleviate this limitation significantly. The GPU also has a limited amount of fast shared memory which can be used to hide the latency of the global memory and to share data between threads within a block in order to save the memory bandwidth. The device also has *registers* and read-only *texture* and *constant memories*. A more accurate description of these can be found in the CUDA programming guide [90, 91]. We have used a range of these memories in order to optimize the execution of the CUDA kernels.

4.2 Lattice simulations

In all of the aforementioned lattice codes the system is discretized and then embedded in a periodic lattice environment. In the CUDAEASY program we used a second-order accurate leap-frog method to evolve the system that has been previously used, for example, in LATTICEEASY [65]. In the following PyCOOL program [5] we resorted to a much more sophisti-

cated symplectic implementation that generally is temporally more precise by orders of magnitude. We will next introduce the main features of this symplectic method of solving evolution of the system.

4.2.1 Symplectic dynamics

Symplectic integrators are frequently used to solve the dynamics of a system when some physical quantity needs to be conserved during the evolution process: for example in the case of celestial mechanics long-term integrations of the solar system are often done with different symplectic integrators. In this thesis symplectic integrators are used to conserve the form of the Friedmann equations (2.9) and (2.13). The accuracy of the method is measured from the amount of accumulated residual curvature which we calculate with Eq. (2.11).

The symplectic method of solving the dynamics during preheating was first developed by A. Frolov and Z. Huang [92]. Overall the scheme follows closely the principles used in different variational integrators [93]. The starting point is the action of the system, which is first discretized spatially to derive the discrete Lagrangian function $\mathcal{L}$. The Hamiltonian of the system is then derived through a Legendre transformation. Lastly the equations of motion are determined from Hamilton's equations.

The action from which the dynamics is determined in general relativity is

$$S = \int \Big(- \frac{\mathcal{R}}{16\pi G} + \mathcal{L}_m \Big) \sqrt{-g}\, \mathrm{d}^4 x, \tag{4.1}$$

where $\mathcal{R}$ is the Ricci curvature scalar and $\mathcal{L}_m$ is the Lagrange function of the matter content of the Universe. The preheating phase is modeled with semi-classical scalar fields that are minimally coupled to gravity and the matter action is hence given by Eq. (2.25).

The space-time is again assumed to be a flat Friedmann-Robertson-Walker universe and we have used conformal time η to have simpler Hamilton's equations. It then follows that the determinant of the metric tensor equals

$$\sqrt{-g} = a^4 \tag{4.2}$$

and the Ricci scalar reads

$$\mathcal{R} = -6 \frac{a''}{a^3}, \tag{4.3}$$

where prime again denotes differentiation with respect to the conformal time.

After doing temporal and spatial partial integrations [5], the action can be written as

$$S = \int \Bigg(- 3a'^2 m_{Pl}^2 V_L (dx)^3 + \int \Big(\sum_i \frac{\phi_i'^2}{2a^2} + \frac{\phi_i \nabla^2 \phi_i}{2a^2} - V(\phi_1, ..., \phi_N) \Big) a^4 \mathrm{d}^3 x \Bigg) \mathrm{d}\eta, \tag{4.4}$$

where the index $i = 1, ..., N$ labels the different fields, ∇ is the gradient operator with respect to comoving coordinates and $V_L = n^3$ is the number of points in the periodic lattice in which the fields are embedded. In order to optimize the GPU implementation, we have also done a spatial partial integration to the gradient terms of the scalar fields to eliminate the computationally difficult $(\nabla\phi)^2$ terms from the evolution equations.

The next step is the spatial discretization of the lattice, where the system in transformed into $i \times n^3$ time dependent, coupled differential equations. In the discretization, integrals transform to spatial summations and the gradient terms are replaced with stencil operators that determine the spatial resolution of the simulation. We have used the second order accurate stencils for the Laplacian terms that were presented in detail in [94]. These were also used in DEFROST [66], CUDAEASY [4] and in the symplectic method of Frolov and Huang [92]. In this notation the Laplacian operator reads

$$D[\phi](x,y,z) = \sum_{i=x-1}^{x+1} \sum_{j=y-1}^{y+1} \sum_{k=z-1}^{z+1} c_{d(i,j,k)} \phi(i,j,k) = \sum_{\alpha} c_{d(\alpha)} \phi(\alpha), \tag{4.5}$$

where $c_{d(\alpha)}$ are the discretization coefficients of the Laplacian [94]. We also have

$$G[\phi](x,y,z) = \frac{1}{2} \sum_{\alpha} c_{d(\alpha)} \Big(\phi(\alpha) - \phi(x,y,z) \Big)^2 \tag{4.6}$$

for $(\nabla\phi)^2$ terms used in the energy density terms [66]. The discretized

action (4.4) then reads

$$\begin{aligned} S =&(\mathrm{d}x)^3 \int \Bigg[- 3a'^2 V_L m_{Pl}^2 + \sum_{\vec{x}} a^2 \Big(\sum_i \Big(\frac{\phi_{i,\vec{x}}'^2}{2} + \frac{\phi_{i,\vec{x}} D[\phi_{i,\vec{x}}](\vec{x})}{2dx^2} \Big) \\ &- a^2 V(\phi_{1,\vec{x}}, ..., \phi_{N,\vec{x}}) \Big) \Bigg] \mathrm{d}\eta \\ =&(\mathrm{d}x)^3 \int \mathcal{L}[a, \phi_1, ...\phi_N] \mathrm{d}\eta, \end{aligned} \tag{4.7}$$

where we have labeled the different scalar fields with the index i and their location in the lattice $\vec{x}$.

In order to determine the Hamiltonian $\mathcal{H}$, the canonical momentum variables have to be determined. From the Lagrangian $\mathcal{L}$ we get for the scale parameter

$$p_a = \frac{\partial \mathcal{L}}{\partial a'} = -6a' V_L m_{Pl}^2 \tag{4.8}$$

and for the field variables

$$\pi_{i,\vec{x}} = \frac{\partial \mathcal{L}}{\partial \phi_{i,\vec{x}}'} = a^2 \phi_{i,\vec{x}}'. \tag{4.9}$$

After a simple Legendre transformation of the Lagrangian, the Hamiltonian function of the system is given by

$$\mathcal{H} = -\frac{p_a^2}{12 V_L m_{Pl}^2} + \sum_{i,\vec{x}} a^4 \left(\frac{\pi_{i,\vec{x}}^2}{2a^6} - \frac{\phi_{i,\vec{x}} D[\phi_{i,\vec{x}}](\vec{x})}{2a^2 dx^2} + V(\phi_{1,\vec{x}}, ..., \phi_{N,\vec{x}}) \right). \tag{4.10}$$

Hamilton's equations now read for the scale parameter

$$\begin{aligned} a' &= \frac{\partial \mathcal{H}}{\partial p_a} = -\frac{p_a}{6 V_L m_{Pl}^2} \\ p_a' &= -\frac{\partial \mathcal{H}}{\partial a} = \sum_{i,\vec{x}} a^3 \left(\frac{\pi_{i,\vec{x}}^2}{a^6} + \frac{\phi_{i,\vec{x}} D[\phi_{i,\vec{x}}](\vec{x})}{a^2 dx^2} - 4V(\phi_{1,\vec{x}}, ..., \phi_{N,\vec{x}}) \right) \end{aligned} \tag{4.11}$$

whereas the equations of motion of scalar field ϕ_i at grid point $\vec{z}$ are

$$\begin{aligned}\phi'_{i,\vec{z}} &= \frac{\partial \mathcal{H}}{\partial(\pi_{i,\vec{z}})} = \frac{\pi_{i,\vec{z}}}{a^2} \\ \pi'_{i,\vec{z}} &= -\frac{\partial \mathcal{H}}{\partial(\phi_{i,\vec{z}})} = a^2 \frac{D[\phi_{i,\vec{z}}](\vec{z})}{dx^2} - a^4 \frac{\partial V}{\partial(\phi_{i,\vec{z}})}.\end{aligned} \tag{4.12}$$

These follow from equation (4.10) by differentiating under the summation sign and by summing over the coefficients $c_{d(\alpha)}$.

The initial values of the system are chosen in such a way that the first Friedmann equation, which we write in discrete form

$$(a')^2 = \frac{a^4}{3m_{Pl}^2}\langle\rho\rangle, \tag{4.13}$$

is satisfied. Note that $\langle\rangle$ denotes averaging over the volume of the lattice. With the total energy density of the scalar fields given by Eq. (2.28) we obtain

$$\frac{p_a^2}{12V_L m_{Pl}^2} = \sum_{i,\vec{x}} a^4 \left(\frac{\pi_{i,\vec{x}}^2}{2a^6} - \frac{\phi_{i,\vec{x}} D[\phi_{i,\vec{x}}](\vec{x})}{2a^2 dx^2} + V(\phi_{1,\vec{x}}, ..., \phi_{N,\vec{x}}) \right), \tag{4.14}$$

where we have also used the definitions of the canonical momenta from Eqs. (4.8) and (4.9). In terms of the Hamiltonian function (4.10), this means that for a solution satisfying the first Friedmann equation, equality $\mathcal{H} = 0$ is satisfied initially. This equality is conserved during time evolution by the symplectic integrator and any deviation from zero is interpreted as a residual curvature term.

The second Friedmann equation is related to dynamics through the equation of motion of p_a. This can be seen by using the total energy density and pressure of the scalar fields from Eq. (2.28) and the equality $a' = -\frac{p_a}{6V_L m_{Pl}^2}$ in the discretized version of the second Friedmann equation

$$a'' = -\frac{a^3}{6m_{Pl}^2}\langle\rho - 3P\rangle, \tag{4.15}$$

which will lead to the equation of motion of p_a.

In the curvaton scenario a homogeneous radiation component originating from the inflaton field is often included in the system. In the Hamiltonian formalism this can be accomplished by adding a term $V_L(\rho_{\gamma,0} + a\rho_{m,0})$ on the right hand side of the Hamiltonian (4.10) which will lead to equations

of motion consistent with the Friedmann equations [5].

4.2.2 Implementation on the GPU

The initial conditions of the scalar fields are set by assuming that the modes that are relevant to the studied process, *e.g.* preheating, never leave the Hubble horizon and are treated as vacuum fluctuations with a spectrum

$$\mathcal{P}_\phi = \frac{1}{2\omega_k}, \tag{4.16}$$

where ϕ is a generic scalar field and $\omega_k^2 = k^2 + m^2$ [41]. We will also assume that the evolution can be solved classically at all times. This becomes a valid assumption rather quickly after the start of the parametric resonance as the occupation numbers of the fields start to grow rapidly [95].

This initialization procedure is implemented with a convolution based method that was presented in DEFROST [66]. The fields are first written as operators as in Eq. (2.48) and the different creation and annihilation operators are treated as complex random variables that satisfy the commutation relations (2.49). The mass term in the dispersion relation can be replaced with an effective term $m_{\text{eff}}^2 = m^2 - \frac{9}{4}H^2$ where H is the Hubble parameter although this term can be often neglected from the expression. The fluctuations are then generated by convolving white noise with a kernel function that produces the required spectrum given by Eq. (4.16) [96, 97].

The symplectic integration of the equations of motion derived from the Hamiltonian (4.10) is done by splitting the Hamiltonian into parts that can be integrated explicitly. A good introduction to the subject of different splitting methods and geometric integrators can be found for example in Ref. [98]. We have used a splitting where the scale factor is evolved first ($\mathcal{H}_1$), scalar fields next by the second Hamiltonian ($\mathcal{H}_2$) and the canonical momenta of the fields in the last part ($\mathcal{H}_3$). The explicit forms of the equations are given in Ref. [5]. The evolution of the scale factor is handled by the CPU whereas the scalar fields and their canonical momenta are handled by the GPU.

We will now go briefly through the steps involved in the GPU evolution. CUDA implementation of the 3D stencils that are needed when the canonical momenta of the fields are updated (see Eq. (4.12)) was presented in detail in [99]. In the program we will use a similar scheme which uses the shared memory to calculate the Laplacian operators. Because of the limited amount of the shared memory on the GPU the 3 dimensional lat-

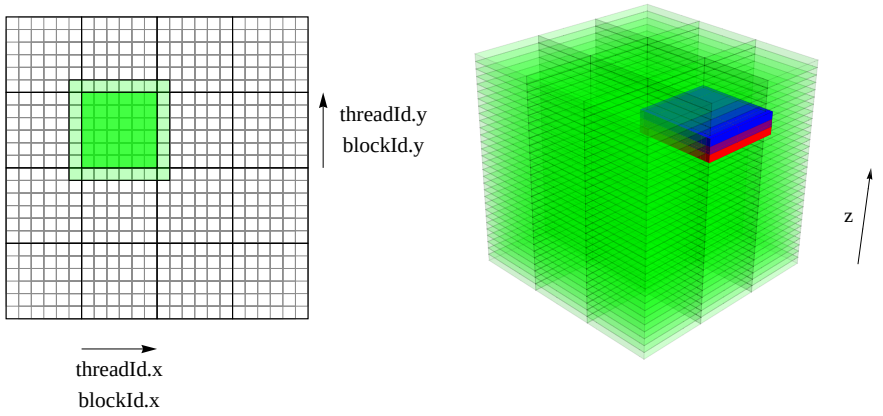

(a) (b)

Figure 4.1: (a) Illustration of the CUDA grid with 16 thread blocks and 64 threads per block. The actual grid used in the program is much larger. The computations are done by the inner threads (green) of a block whereas the outer threads (light green) are used only to read data. Note that the thread blocks intersect each other. (b) Illustration of how data in the shared memory is updated. Thread blocks advance in the z-direction and load data into the blue slice (shared_up) from the global memory. The previous values of the blue slice are stored into the purple one (shared_middle) and the values from the middle slice are stored into the red block (shared_down). This way only a fraction of the memory bandwidth is needed. Figures taken from Ref. [4].

tice has been divided into more manageable smaller pieces. To accomplish this we slice the lattice along the z-axis into smaller tiles and advance the computation in z-direction. The calculations within these tiles are done by CUDA thread blocks which means that a single thread of a thread block will advance all the scalar fields of a column with constant x- and y-coordinates. Since the outer threads of a thread block need the values of scalar fields that are in a different block and since different blocks can only communicate through global memory the role of the outer threads of a thread block is only to load data into shared memory and the scalar field computations are done by the inner threads. The computation starts from the bottom of the lattice *i.e.* at $z = 0$ and proceeds to the top. We have illustrated this in Fig. 4.1. Note that we have also implemented a slightly more advance version of this method in PyCOOL where all the threads do the computa-

tions with a more complex way of loading the data to the chip. This will in general lead to some speed increase ($\sim 10 - 20\%$) when compared to the method presented here. The newer version has been developed specifically for a future multi-GPU implementation of the code.

The integration of $\phi_{i,\vec{x}}$ does not include any stencil operations (see Eq. (4.12)) that makes this step computationally much easier. Summations over the lattice that are needed when updating p_a are performed also on the GPU and are done simultaneously with the evolution steps of $\phi_{i,\vec{x}}$ and $\pi_{i,\vec{x}}$. The energy density and pressure of the scalar fields are also calculated on the GPU. However since the symplectic evolution equations do not explicitly depend on these variables they are not calculated at every step. This way the number of times the computationally demanding $G[\phi_{i,\vec{x}}]$ terms given in equation (4.6) need to be calculated can be reduced significantly.

4.2.3 Chaotic inflation

We will next present the main simulation results of the simple chaotic inflation model with a potential function

$$V(\phi, \psi) = \frac{1}{2}m^2\phi^2 + \frac{1}{2}g^2\phi^2\psi^2, \tag{4.17}$$

where ϕ is the inflaton field and ψ the decay product, to complete the discussions of Sec. 2.6.2. Notably this model has become a standard test scenario that has been solved previously with LATTICEEASY [46], DEFROST [66] and PSpectRe [67] programs. We also verified the functionality of CUDAEASY [4] and PyCOOL [5] codes with this model and found that in both cases the results are in line with the previous studies. As the symplectic method is much more accurate, the computations we present here have been done using the PyCOOL program. A more thorough examination of the model can be found in Refs. [46, 66].

The initial values have been set to coincide with the values given in [46, 66]. This means that the homogeneous value of the inflaton is set to $\phi \simeq 1.009343$ and the decay field $\psi = 0$, the mass of the inflaton equals $5 \cdot 10^{-6} m_{\rm pl}$, the Hubble parameter $H \simeq 0.50467m$, and the value of the coupling constant is $g = 100m$. With these values $q = \frac{g^2\Phi^2}{4m^2} \gg 1$ and the preheating process is hence very efficient. We have evolved the system with conformal time step $d\eta = 0.0001/m$ and lattice size 256^3 until $t_{\rm phys} = 250/m$ with a fourth order accurate symplectic integrator. We scale the conformal time step with the scale factor a during the simulation which corresponds to an almost constant physical time step. Note that the evolution could be

also solved directly using physical time. This feature has not been, however, yet implemented in the PyCOOL program.

The numerical results are shown in Figs. 4.2(a) -4.2(d). The oscillating inflaton field dominates the energy content at early times meaning that the Universe is on average matter-dominated. This can be seen in Fig. 4.2(a) where we have plotted the evolution of $a^{-3/2}H^{-1}$ as a function of the scale parameter. In a non-relativistic matter dominated universe, $H^2 \propto a^{-3}$, in which case this quantity is a constant. At $a \sim 20$ the system can be seen to become radiation dominated ($H^2 \propto a^{-4}$) as the contribution of the ψ field starts to grow during the re-scattering period [46, 66].

The accuracy of the PyCOOL program is presented in Fig. (4.2(b)) where we plot the absolute value of the relative residual curvature

$$\frac{K}{a^2H^2} = \left|\frac{8\pi G\langle\rho\rangle}{3H^2} - 1\right| \tag{4.18}$$

which quantifies the conservation of the Hamiltonian. When compared to the accuracies of the Defrost and PSpectRe programs [67] PyCOOL is more than 5 orders of magnitude more precise.

The essential features of the resonance process can be seen in Figs. 4.2(c) and 4.2(d) where we plot the evolution of the energy density spectra, ρ_k, of the scalar fields, as defined in Ref. [6]. This is calculated as $\rho_k = \omega_k n_k$, where n_k is the number density spectra of the field and $\omega_k^2 = k^2 + a^2 m_{\rm eff}^2$ is the comoving dispersion relation. Note that in these figures the color evolves with time and the red curves are calculated close to the end of the simulation ($t_{\rm phys} = 250/m$) whereas the blue ones (at the bottom) are evaluated at $t_{\rm phys}\, m = 0$. From these spectra it can be seen that the preheating process first excites modes of the ψ field with $k/m < 20$. These will then back-react with the inflaton field leading to the re-scattering phase of the system [46]. As time progresses also the ultra-violet modes will become excited. The final state of the inflaton field could be characterized as a pre-thermalized one [46]. Eventually the simulation will reach the spatial resolution limit of the lattice as the Universe expands sufficiently. Note also that we have included a visualization of the preheating process on the cover of this thesis where we plot the canonical momentum of the ϕ field at the start of re-scattering phase in shades of blue. Further plots of the resonance process in the current model can be found *e.g.* in Refs. [4, 5, 46, 66].

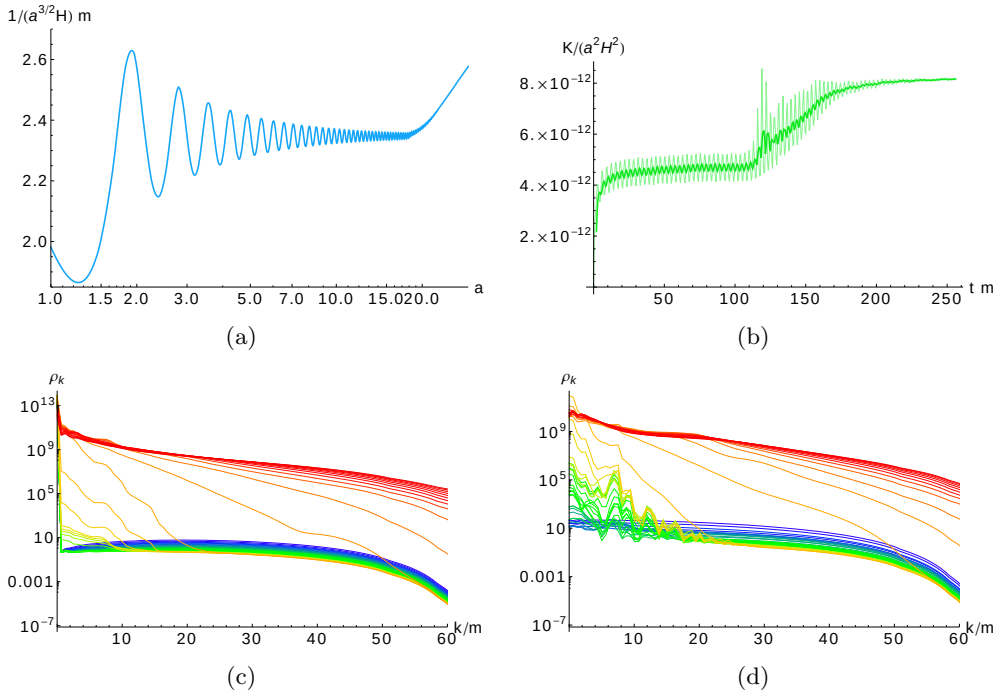

Figure 4.2: (a) The evolution $1/(a^{3/2}H)$ as a function of the scale parameter in the chaotic potential model. (b) The absolute value of the relative residual curvature (4.18) as a function of physical time in units of $1/m$. Note that we use $t\,m$, a dimensionless quantity, as the time variable. The energy density spectrum of (c) ϕ field and (d) ψ field in terms of the comoving momenta. These are calculated from $\rho_k = \omega_k n_k$, where n_k is the number density spectra of the field and ω_k is the comoving dispersion relation, as defined in Ref. [6]. Note that in the last two figures the color evolves with time and the red curves are calculated close to the end of the simulation ($t_{\rm phys} = 250/m$) whereas the blue curves (at the bottom) are evaluated at $t_{\rm phys}\,m = 0$. Note also that the results have been calculated with the PyCOOL program.

Chapter 5

Non-Gaussianity

Cosmological observations are consistent with the hypothesis that the primordial perturbations are Gaussian to a high degree. To quantify this the non-Gaussianity parameter $f_{\rm NL}$ is usually defined as an ansatz [21]

$$\Phi = \Phi_{\rm L} + f_{\rm NL} \star \Phi_{\rm L}^2 \tag{5.1}$$

where Φ is the non-linear Bardeen potential and $\Phi_{\rm L}$ is the linear, Gaussian part defined in Eq. (3.10). Here the star, $\star$, denotes that the non-Gaussianity is calculated actually as convolution that makes it also scale dependent. This quantity can be connected to temperature fluctuations of the CMB radiation through a variant of the Sachs-Wolfe effect $\Delta T/T = -\Phi/3$ and then compared to the values given by a cosmological model. The observational limits are, however, typically given as scale independent pure numbers and in this thesis we will mostly concentrate on this simpler case by using the ansatz

$$\Phi = \Phi_{\rm L} + f_{\rm NL}\Phi_{\rm L}^2. \tag{5.2}$$

Due to new observations [21, 25, 100, 101], that have made it possible to study the statistics of the perturbations, non-Gaussianity has been a popular topic in cosmology in the last ten years. A review of the subject can be found for example in Ref. [21].

In this thesis the generation of non-Gaussianity has been studied in the curvaton model from two complementary angles: perturbatively and through lattice simulations. The methods used in these cases differ quite significantly and we will next present the main features. The basic definition of non-Gaussianity is, however, essentially given by Eq. (5.1) in these both cases.

5.1 Perturbative decay

To calculate the level of non-Gaussianity in the perturbative case, it is necessary to consider the temperature perturbations of the CMB radiation from which the large scale non-Gaussianity can be determined. We have done this with the second order perturbation theory that was presented in section 3.1.5. We follow the notation of Ref. [102] and use the Poisson gauge in the calculations. We are now interested only in the large-scale non-Gaussianities meaning that some terms from the full expression can be safely ignored [102]. We are also interested only in the primordial values of the variables and hence the integrated Sachs-Wolfe effect can be neglected. The temperature fluctuations can be written in this approximation [21] as

$$\frac{\Delta T}{T} = \left[\phi^{(1)} + \tau^{(1)} + \frac{1}{2}\left(\phi^{(2)} + \tau^{(2)}\right) - \frac{1}{2}\left(\phi^{(1)}\right)^2 + \phi^{(1)}\tau^{(1)}\right]_{\mathrm{Em}}, \tag{5.3}$$

where $\phi^{(r)}$ are the metric lapse functions, $\tau = \tau^{(1)} + \frac{1}{2}\tau^{(2)}$ is the intrinsic fractional temperature fluctutation $\tau = \Delta T/T|_{\mathrm{Em}}$ and all the terms are evaluated at the time of emission of the CMB radiation.

It is instructive to define variables that relate the final values of perturbations to their initial values:

$$\begin{aligned} r_1 &= \frac{\zeta_m^{(1)}|_m}{\zeta_{\sigma,\mathrm{in}}^{(1)}}, \quad q_1 = \frac{\zeta_\gamma^{(1)}|_m}{\zeta_{\sigma,\mathrm{in}}^{(1)}} \\ r_2 &= \frac{\zeta_m^{(2)}|_m}{(\zeta_{\sigma,\mathrm{in}}^{(1)})^2}, \quad q_2 = \frac{\zeta_\gamma^{(2)}|_m}{(\zeta_{\sigma,\mathrm{in}}^{(1)})^2}, \end{aligned} \tag{5.4}$$

where we have assumed that the system consists of three fluids as in the three fluid curvaton model. We denote the curvaton component by subscript (σ), radiation by (γ) and cold dark matter by (m) and the different numerators are evaluated at the time of decoupling, when the Universe is matter dominated and hence $\zeta^{(i)} \simeq \zeta_m^{(i)}$. The system is adiabatic if $q_1 = r_1$ and $q_2 = r_2$. In essence these variables tell how efficiently the system can convert the initial curvature perturbations into the matter and radiation components.

To calculate the non-Gaussianity parameter, f_{NL}, Eq. (5.3) needs to be written in terms of the lapse functions, $\phi^{(r)}$. By calculating curvature perturbations in a matter dominated universe, using the perturbed Einstein equations *i.e.* Eq. (3.35) and Eq. (5.4), we can write [2] $\phi^{(2)}$ in a matter

dominated universe in the form

$$\begin{aligned}\phi^{(2)} =&\Big[\frac{16}{3}-\frac{5}{3}\frac{r_2}{r_1^2}\Big](\psi^{(1)})^2+2\nabla^{-2}\Big(\partial^i\psi^{(1)}\partial_i\psi^{(1)}\Big)\\&-6\nabla^{-4}\Big(\partial^i\partial_j\Big(\partial_i\psi^{(1)}\partial^j\psi^{(1)}\Big)\Big),\end{aligned}\tag{5.5}$$

where the inverse Laplacians are implicit integral expressions that have not been written open. In this thesis we are mainly interested in the local form of the non-gaussianity in which these position dependent operators can be neglected. The intrinsic fractional temperature fluctuations $\tau^{(r)}$ can be calculated from $\rho_\gamma \propto T^4$ by expanding this to second order and using equality $\phi^{(1)} = -3\zeta^{(1)}/5$, which is valid in a matter-dominated universe [103].

Combining all of the above expressions for perturbations and substituting into the equation for the temperature fluctuations (5.3) one finally has [2]

$$\begin{aligned}\frac{\Delta T}{T} =&\frac{6r_1-5q_1}{3r_1}\Big[\phi^{(1)}\\&+\Big[\frac{25(q_2-q_1^2)-60q_1r_1+96r_1^2-30r_2}{6r_1(6r_1-5q_1)}\Big]\Big(\phi^{(1)}\Big)^2\Big]\\&+\frac{1}{3}\nabla^{-2}\Big(\partial^i\psi^{(1)}\partial_i\psi^{(1)}\Big)-\nabla^{-4}\Big(\partial^i\partial_j\Big(\partial_i\psi^{(1)}\partial^j\psi^{(1)}\Big)\Big),\end{aligned}\tag{5.6}$$

where we have ignored the momentum dependent terms because we are interested in the large scale non-Gaussianity [21]. From Eq. (5.6) we can read that in the adiabatic limit, *i.e.* $r_1 = q_1$ and $r_2 = q_2$, we recover at second order an extension of the first order Sachs-Wolfe effect $\Delta T/T = \phi^{(1)}/3$ given in [21]:

$$\frac{\Delta T}{T} =\frac{1}{3}\Big[\phi^{(1)}+\frac{1}{2}\Big(\phi^{(2)}-\frac{5}{3}\big(\phi^{(1)}\big)^2\Big)\Big].\tag{5.7}$$

In the opposite case of pure isocurvature perturbation, equation (5.6) is not valid since we have assumed that $r_1 \neq 0$ and for isocurvature perturbations $0 = \zeta^{(1)}\Big|_{Dec} \simeq \zeta_m^{(1)}\Big|_{Dec} = r_1\zeta^{(1)}_{\sigma,\mathrm{in}}$.

We can now define the non-Gaussianity parameter f_{NL} in the general case. Following the notation of [104] we write the temperature fluctuations in the form

$$\frac{\Delta T}{T} = g_T\Big[\phi^{(1)}+f_{NL}\big(\phi^{(1)}\big)^2\Big],\tag{5.8}$$

where the factor g_T depends on the state of the system *e.g.* for a completely adiabatic one $g_T = 1/3$ and in our calculations $g_T = (6r_1 - 5q_1)/(3r_1)$. We have ignored the gradient terms from our definition of non-Gaussianity but when calculating the bispectrum they need to be included. Note that this definition leads to a sign difference when compared to the usual approach using the Bardeen potential [21]. Now from equation (5.6) we can easily read off the non-Gaussianity parameter

$$f_{NL} = \frac{25(q_2 - q_1^2) - 60q_1r_1 + 96r_1^2 - 30r_2}{6r_1(6r_1 - 5q_1)}, \tag{5.9}$$

which is well defined since $r_1 \neq 0$ and $q_1 \leq r_1$.

5.2 Non-Gaussianity from preheating

The generation of non-Gaussianity during the preheating and resonance process has been analyzed previously in Refs. [105–111]. As was shown in Ref. [108], to calculate the non-Gaussianity parameter accurately in the non-perturbative case, the evolution of the scalar fields needs to be solved also inside the Hubble horizon. This is done with the ΔN formalism in conjunction with a separate universe approach [112] that have been previously applied successfully to different parametric resonance scenarios [108–111]. In the separate universe approach different patches of the universe that are separated by more than a Hubble distance are presumed to evolve independently of each other. Assuming also that each Hubble volume is isotropic and homogeneous they can be approximated to be separate Friedmann-Robertson-Walker 'universes'. The evolution of these patches is solved with the lattice simulation method presented in Chapter 4.

5.2.1 ΔN formalism

The curvature perturbation on scales larger than the Hubble horizon is defined as [113]

$$\zeta = \delta \ln a|_H, \tag{5.10}$$

where the difference in the scale factor is calculated at a hypersurface of constant Hubble parameter H. The scale factor is set to one at the start of thermalization process. The homogeneous values of the field σ are varied with superhorizon fluctuations from one patch to another. This will cause slight variations in the value of the curvature perturbation ζ. For small field

perturbations $\delta\sigma$ equation (5.10) is expanded as

$$\zeta = (\ln a)'\Big|_H \delta\sigma + \frac{1}{2}(\ln a)''\Big|_H \delta\sigma^2 + \dots, \tag{5.11}$$

where the primes are derivatives calculated with respect to the field value at the end of inflation on hypersurfaces of constant Hubble parameter H. The spectrum of the curvature perturbation can be written using Eq. (5.11) as

$$\mathcal{P}_\zeta = \Big[(\ln a)'\Big]^2 \mathcal{P}_\sigma, \tag{5.12}$$

where $\mathcal{P}_\sigma$ is the spectrum of the scalar field σ.

To define the local non-Gaussianity parameter we write Eq. (5.2) in terms of the curvature perturbation ζ as

$$\zeta = \zeta_{\mathrm{L}} + \frac{3}{5} f_{\mathrm{NL}} \zeta_{\mathrm{L}}^2 + \mathcal{O}(\zeta_{\mathrm{L}}^3) \tag{5.13}$$

where we have used the equality $\phi^{(1)} = -3\zeta^{(1)}/5$, which is valid in a matter dominated universe [103] and changed the sign of f_{NL} compared to Eq. (5.2). Note that here ζ_{L} is the linear part of curvature perturbation. The local non-Gaussianity parameter then reads in terms of the coefficients of equation (5.11) [103] as

$$f_{\mathrm{NL}} = \frac{5}{6} \frac{(\ln a)''}{((\ln a)')^2}\bigg|_H . \tag{5.14}$$

5.2.2 Curvaton scenario

To calculate the non-Gaussianity in the curvaton scenario we will resort to approximative methods. Following Ref. [111] we will treat the curvaton component as a subdominant non-relativistic matter fluid after the resonance process is over and assume that it decays perturbatively into radiation when $H \sim \Gamma$, where Γ is an unknown decay width of the curvaton. We employ the sudden decay approximation identically to Sec. 3.2.2 to make the analytical calculations simpler.

To proceed we write the energy density as a combination of the relativistic radiation and the curvaton component which we assume to behave like non-relativistic matter

$$\rho = \rho_{\mathrm{ref}} \Big[r_{\mathrm{ref}} \Big(\frac{a}{a_{\mathrm{ref}}} \Big)^3 + (1 - r_{\mathrm{ref}}) \Big(\frac{a}{a_{\mathrm{ref}}} \Big)^4 \Big], \tag{5.15}$$

where the fractional energy density of curvaton $r_{\rm ref} = \Omega_{\sigma,\rm ref}$, scale factor $a_{\rm ref}$ and the energy density $\rho_{\rm ref}$ are calculated at some reference point well after the resonance process is over. By now taking the logarithm of both sides of equation (5.15), expanding the right hand side in series with respect to $r_{\rm ref}$ and rearranging the terms we obtain

$$\begin{aligned}\ln a =& \ln a_{\rm ref} + \frac{1}{4}\left[\ln\frac{\rho_{\rm ref}}{\rho} + r - r_{\rm ref}\right] \\ =& \ln a_{\rm ref} + \frac{1}{4}\left[\ln\frac{\rho_{\rm ref}}{\rho} + C r_{\rm ref}\right],\end{aligned} \tag{5.16}$$

where

$$r \equiv r_{\rm ref}\left(\frac{\rho_{\rm ref}}{\rho}\right)^{1/4} \tag{5.17}$$

and $C \equiv r/r_{\rm ref} - 1$. The curvature perturbation can then be written as

$$\zeta(\hat{\sigma}_0) = \ln a(\hat{\sigma}_0) - \ln a(\sigma_0) = \delta \ln a_{\rm ref} + C\delta r_{\rm ref} \tag{5.18}$$

where we have written explicitly the dependence on the curvaton value at the end of inflation. We have also neglected the energy density terms from equation (5.16) since the calculations are done on a constant H hypersurface (on which the energy density is also constant by the Friedmann equations).

To calculate the level of non-Gaussianity we differentiate Eq. (5.16) with respect to the field value on the constant H hypersurface. This leads to

$$\begin{aligned}(\ln a)'\Big|_H =& (\ln a_{\rm ref})' + \frac{(r_{\rm decay} - r_{\rm ref})}{4}\frac{r'_{\rm ref}}{r_{\rm ref}} \\ (\ln a)''\Big|_H =& (\ln a_{\rm ref})'' + \frac{(r_{\rm decay} - r_{\rm ref})}{4}\frac{r''_{\rm ref}}{r_{\rm ref}},\end{aligned} \tag{5.19}$$

where $r_{\rm decay}$ is the curvaton fractional energy density at the moment of decay. In the derivation we have assumed that the total energy densities $\rho_{\rm ref}$ and $\rho_{\rm decay}$ are fixed and hence independent of the curvaton fluctuation value. With these equations we can solve $r_{\rm decay}$ in terms of field spectra by using Eq. (5.12)

$$r_{\rm decay} = r_{\rm ref} + 4\frac{r_{\rm ref}}{r'_{\rm ref}}\left(\pm\sqrt{\frac{\mathcal{P}_\zeta}{\mathcal{P}_\sigma}} - (\ln a_{\rm ref})'\right), \tag{5.20}$$

where $\mathcal{P}_\zeta \simeq 2.4 \times 10^{-9}$ is the amplitude of the curvature perturbation spectrum (5.12) given by WMAP observations [24]. The non-Gaussianity parameter (5.14) can be then written as [111]

$$f_{\rm NL} = \frac{5}{6}\frac{\mathcal{P}_\sigma}{\mathcal{P}_\zeta}\left((\ln a_{\rm ref})'' + \frac{r''_{\rm ref}}{r'_{\rm ref}}\left(\pm\sqrt{\frac{\mathcal{P}_\zeta}{\mathcal{P}_\sigma}} - (\ln a_{\rm ref})'\right)\right). \tag{5.21}$$

To calculate these variables from the simulation data we will assume that the logarithm of the scale factor and the fractional energy density can be expanded in terms of the superhorizon fluctuations of the homogeneous curvaton values, similarly to equation (5.11):

$$\begin{aligned} \ln a_{\rm ref}(\hat{\sigma}_0) =& \ln a_{\rm ref}(\sigma_0) + (\ln a_{\rm ref})'(\hat{\sigma}_0 - \sigma_0) \\ &+ \frac{1}{2}(\ln a_{\rm ref})''(\hat{\sigma}_0 - \sigma_0)^2, \\ r_{\rm ref}(\hat{\sigma}_0) =& r_{\rm ref}(\sigma_0) + r'_{\rm ref}(\hat{\sigma}_0 - \sigma_0) \\ &+ \frac{1}{2}r''_{\rm ref}(\hat{\sigma}_0 - \sigma_0)^2, \end{aligned} \tag{5.22}$$

where $\hat{\sigma}_0 = \sigma_0 + \delta\sigma_0$ and $\delta\sigma_0$ is a superhorizon fluctuation of the initial curvaton value. Equations (5.22) are then fitted to the simulation data (calculated with different values of $\hat{\sigma}_0$) to get numerical values for the polynomial coefficients $(\ln a_{\rm ref})'$, $(\ln a_{\rm ref})''$, $r'_{\rm ref}$ and $r''_{\rm ref}$ which are then used in Eqs. (5.20) and (5.21) to compute the non-Gaussianity parameter.

The range of homogeneous curvaton values over which the simulations need to be run is determined by the variance of the curvaton values at the end of inflation. This can be written in terms of the spectrum as

$$\langle \delta\sigma^2 \rangle = \int_{a_0 H_0}^{aH} \mathcal{P}_\sigma \frac{dk}{k}, \tag{5.23}$$

where a_0 and H_0 are the current values of the scale factor and the Hubble parameter respectively, whereas the upper limit is calculated at the start of the simulation. Assuming that the inflation potential is $V = \frac{1}{4}\lambda\phi^4$ the curvaton spectrum reads [111]

$$\mathcal{P}_\sigma(k) \approx \frac{H_k^2}{4\pi^2} \approx \frac{4}{3\pi^2}\lambda m_{\rm Pl}^2 N_k^2, \tag{5.24}$$

which is valid for massless fields during inflation. $N_k (\approx 60)$ here measures the number of e-foldings before the $k = aH_k$ mode left the Hubble horizon

end of inflation. The variance is then given by [111]

$$\langle \delta\sigma^2 \rangle \approx \frac{4}{9\pi^2} \lambda m_{\mathrm{Pl}}^2 N_0^3 \tag{5.25}$$

where $N_0 \approx 60$ is the number of e-foldings after the largest currently observable scales left the horizon. The range of curvaton initial values is given by

$$\sigma_0 - \frac{1}{2}\delta\sigma_0 \leq \hat{\sigma}_0 \leq \sigma_0 + \frac{1}{2}\delta\sigma_0, \tag{5.26}$$

where $\delta\sigma_0 = \sqrt{\langle \delta\sigma^2 \rangle}$. The homogeneous curvaton field value, $\hat{\sigma}_0$, is drawn from a Gaussian distribution which variance [111] depends on the total number of e-foldings of inflation, meaning that its value can be chosen almost freely. In the simulations that were done in Ref. [6] the value was chosen based on two criteria: a quartic self-interaction term was assumed to dominate the curvaton potential and the resonance band of particle creation needed to be inside the lattice.

To calculate the non-Gaussianity we take a number of equidistant points from the given range and use as the initial homogeneous curvaton values in the simulations. At each point the evolution is solved multiple times with different random field perturbations to get the necessary statistics for f_{NL} parameter.

Chapter 6

Results and conclusions

In this thesis we have approached the curvaton scenario from a number of different perspectives with perturbative and non-perturbative methods. In this chapter we will summarize these results after which we end this introductory part with an outlook for the topics we have discussed.

6.1 Summary of the research articles

We have divided the results in chronological order and further separated them into perturbative and non-perturbative decay cases.

6.1.1 Perturbative decay

In research papers [1–3] the emphasis is on different variations of a three fluid curvaton model in which the curvaton decays into both radiation and cold dark matter (CDM). The main focus is on the physicality of the model in terms of the temperatures that are achieved at the moment of Big Bang Nucleosynthesis (BBN), radiation-matter equality and decoupling. In the latter papers we also used the level of non-Gaussianity as an additional constraint on the model.

In the first research paper [1] we focused for the most part on the physicality of the solutions in terms of the temperatures at the different epochs of the early Universe. We scanned systematically the parameter space and identified those regions where the physicality criteria are met. The main conclusion was that if the decay rates are comparable to the Hubble rate, a small initial curvaton density is required. Otherwise one needs to fine-tune the decay rates to be much smaller than H at the onset of the decay. If the

isocurvature $S_{\mathrm{m}\gamma} = 3(\zeta_{\mathrm{m}} - \zeta_\gamma)$ is also included in the analysis this reduces the physically sound parameter regions even further.

In the second paper [2] we studied the generation of non-Gaussianity in the curvaton model of the first study. The main result was the derivation of the non-Gaussianity formula (5.9) which we then applied to the curvaton model. The most interesting observation was that in the three fluid curvaton model the level of non-Gaussianity produced was found to be small ($|f_{NL}| \sim \mathcal{O}(1)$). This should be compared to the two fluid curvaton model, where much larger non-Gaussianities are easily produced (*i.e.* $|f_{NL}| \sim \mathcal{O}(10)$ or even $\sim \mathcal{O}(100)$) [21, 100]. This result can be understood in terms of how efficiently the system can generate matter perturbations [21]: in the two fluid system we can easily have $r_1 = \zeta_m^{(1)}|_m/\zeta_{\sigma,\mathrm{in}}^{(1)} < 1$ and since the observed level of perturbations has to stay constant, the lower efficiency generally means greater non-Gaussianity. However in the three fluid model the system is always perfectly efficient ($r_1 = 1$) due to a conserved quantity

$$\rho_{\mathrm{comp}} = \rho_m + \frac{\Gamma_m}{\Gamma_\gamma + \Gamma_m}\rho_\sigma. \tag{6.1}$$

A universe with low observed non-Gaussianity is most often associated with a simple single field inflaton model [21]. We hence showed even in this case that the curvaton scenario is a viable alternative interpretation.

In the last of the perturbative papers [3] we altered the premise of the curvaton scenario by assuming that the equation of state of the dark matter (DM) component evolves with time. This was done by evolving explicitly the temperature of the dark matter in the numerical computations. Initially DM was presumed to be relativistic and only after the expansion of the Universe had reduced its temperature it became non-relativistic. Notably this means that the system is no longer always perfectly efficient ($r_1 = 1$) as ρ_{comp} is not conserved. In this case we focused on the physicality of the system and the generation of non-Gaussianities. We found that the non-Gaussianity generated in the system can be considerable but these large values are reached with initial values that do not lead to physically sound temperatures for the system during nucleosynthesis and radiation-matter equality. The non-Gaussianity is therefore expected to be of the same order of magnitude as in the simple inflaton models [21]. The curvaton model was found to lead to evolution in agreement with the temperature limits of standard cosmology with different values of the dark matter particle mass, m_m. Lower initial temperatures and mass m_m generally permitted greater decay rates.

6.1.2 Non-perturbative decay

The fourth and fifth research papers [4, 5] were devoted almost completely to the development of CUDAEASY and PyCOOL programs, the main features of which were discussed in Chapter 4. In essence I was able to herald the computational methods that are needed in different preheating and resonance scenarios to a new era in terms of speed, accuracy, ease of usage and computing platform.

In the last research paper [6] these advances were put to use and applied to the parametric resonance of a self-interacting curvaton field. I first verified that the results are in line with previous studies of self-interacting scalar fields [95, 114]. More specifically during the resonance period curvaton particles were found to be created at a predicted resonance band and in the ensuing rescattering phase the spectrum was found to develop peaks at harmonic frequencies related to the momentum values of the band.

I then focused on the generation of non-Gaussianity during the resonance process by employing and adapting the methods presented in Sec. 5.2 to the self-interacting curvaton scenario. When compared to the broad resonance of the curvaton [111] the simulation data were found to be a better fit to the quadratic approximation of the curvature perturbation given in Eq. (5.11). The level of non-Gaussianity was found to be very high, $f_{\mathrm{NL}} \sim \mathcal{O}(1000)$, and in conflict with current observational limits [25] $-9 < f_{\mathrm{NL}} < 111$ at 95% confidence level. It should be noted that the simulations were run only with a single set of parameters in the paper. More comprehensive study of the parameter space could lead to the discovery of areas where the level of non-Gaussianity could be substantially lower and in agreement with observations. The process could also lead to a spikey pattern that was observed in Ref. [110]. The study of these aspects would, however, demand substantial computational resources.

6.2 Conclusions and outlook

During the last few decades our picture of the Universe and its history has changed quite drastically, in large part due to different groundbreaking observational programs. Despite the many advancements numerous aspects of the early Universe remain unclear. These include questions about the correctness of the inflation theory, the origin of the baryon asymmetry and the nature of the dark energy.

The curvaton hypothesis that has been explored in this thesis is one explanation for the origin of the structure of the Universe we see today.

During the last ten years it has been been studied extensively and today it is seen as a well motivated alternative to the standard inflation scenario. In this thesis we have presented our contribution to its analysis and comprehension by approaching it via different physicality constraints and through the level of non-Gaussianity it can generate.

The results for the amount of produced non-Gaussianity were found to be quite different in the perturbative reheating and non-linear preheating scenarios studied. On one hand, in the perturbative case the non-Gaussianity parameter, $f_{\rm NL}$, was found to be very small on the condition that the curvaton is responsible for the cold dark matter component of the Universe. On the other hand, in the studied preheating scenario of the curvaton model the level of non-Gaussianity was found to be quite large and ruled out by current observational limits. Direct comparison of these results might, however, be troublesome because in the linear case the evolution of the system was solved using a large number of different initial and parameter values whereas in the non-linear case the non-Gaussianity parameter was computed using only a single set of initial values. In the preheating study the curvaton field was, in addition, assumed to decay only into radiation and no dark matter component was included in the analysis. Notably a similar premise in the perturbative decay scenario can also produce large levels of non-Gaussianity. Previous studies of different preheating scenarios [105–111] have, however, also found similarly large values of non-Gaussianity, indicating that the non-linear resonance period can rather easily lead to very large values of $f_{\rm NL}$.

This naturally raises the question of whether the large levels of non-Gaussianity are a general property of the preheating process and is fine-tuning needed to be within the limits given by the CMB radiation. As was shown in Ref. [108] the study of this needs to be performed with the methods presented in Sec. 5.2, *i.e.* with the separate universe approach and lattice simulations. The computations could be done, for example, with the fast and accurate PyCOOL program that I developed in this thesis. The number of simulations that needs to be performed is, however, substantial ($\gtrsim 10^2$) even for a single choice of the parameters. To scan systematically the parameter space would therefore either need significant computational resources or some simplifications to the premise of the numerical calculations. One choice would be to use two dimensional simulations and study how close the results are to those given by the full 3D computations. The timeliness of this sort of non-Gaussianity study is highlighted by the Planck mission [11] which is expected give much more strict limits on the non-

Gaussianity parameter f_{NL} in the near future.

Even if the curvaton hypothesis, which has been the central theme of this thesis, proves to be an inaccurate description for Nature, the methods and programs that have been developed can still be used to understand various aspects of the primordial Universe, especially in different models of the non-linear resonance process. Traditionally the evolution in this case has been solved numerically using expensive cluster computers. With the programs developed in this thesis it is now possible to do these computations in many instances using much cheaper common desktop computers without needing to sacrifice the accuracy or the speed of the simulations. Hopefully the work done in this thesis will play a part in the quest to gain a clearer understanding of the dawn of the Universe and, more importantly, in the pursuit to find a better answer to the age-old question: "Mommy, Daddy, how come somethings are and somethings are not and where did everything come from?"

Bibliography

[1] T. Multamäki, J. Sainio, and I. Vilja, *Constraints on the three-fluid model of curvaton decay*, Int. J. Mod. Phys. **D18** (2009) 2047–2059, [arXiv:0710.0282].

[2] T. Multamäki, J. Sainio, and I. Vilja, *Non-Gaussianity in three fluid curvaton model*, Phys. Rev. **D79** (2009) 103516, [arXiv:0803.2637].

[3] J. Sainio and I. Vilja, *Curvaton decay into relativistic matter*, Phys. Rev. **D81** (2010) 083516, [arXiv:0912.3394].

[4] J. Sainio, *CUDAEASY - a GPU Accelerated Cosmological Lattice Program*, Comput. Phys. Commun. **181** (2010) 906–912, [arXiv:0911.5692].

[5] J. Sainio, *PyCOOL - a Cosmological Object-Oriented Lattice code written in Python*, JCAP **1204** (2012) 038, [arXiv:1201.5029].

[6] J. Sainio, *Curvaton preheating revisited*, Phys. Rev. **D85** (2012) 123515, [arXiv:1203.5316].

[7] A. Einstein, *Die Feldgleichungen der Gravitation*, Sitzungsberichte der Preussischen Akademie der Wissenschaften zu Berlin (1915) 844–847.

[8] E. Hubble, *A relation between distance and radial velocity among extra-galactic nebulae*, Proceedings of the National Academy of Sciences **15** (1929), no. 3 168–173, [http://www.pnas.org/content/15/3/168.full.pdf+html].

[9] D. Fixsen, E. Cheng, J. Gales, J. C. Mather, R. Shafer, et al., *The Cosmic Microwave Background spectrum from the full COBE FIRAS data set*, Astrophys. J. **473** (1996) 576, [astro-ph/9605054].

[10] C. Bennett et al., *The Microwave Anisotropy Probe (MAP) mission*, Astrophys. J. **583** (2003) 1–23, [astro-ph/0301158].

[11] P. Ade et al., *Planck Early Results. I. The Planck mission*, Astron. Astrophys. **536** (2011) 16464, [arXiv:1101.2022].

[12] A. H. Guth, *The Inflationary Universe: A Possible Solution to the Horizon and Flatness Problems*, Phys. Rev. **D23** (1981) 347–356.

[13] K. Sato, *First Order Phase Transition of a Vacuum and Expansion of the Universe*, Mon.Not.Roy.Astron.Soc. **195** (1981) 467–479.

[14] A. Starobinsky, *A new type of isotropic cosmological models without singularity*, Physics Letters B **91** (1980), no. 1 99 – 102.

[15] A. Linde, *A new inflationary universe scenario: A possible solution of the horizon, flatness, homogeneity, isotropy and primordial monopole problems*, Physics Letters B **108** (1982), no. 6 389 – 393.

[16] A. D. Linde, *Chaotic Inflation*, Phys. Lett. **B129** (1983) 177–181.

[17] V. F. Mukhanov and G. Chibisov, *Quantum Fluctuation and Nonsingular Universe. (In Russian)*, JETP Lett. **33** (1981) 532–535.

[18] A. H. Guth and S. Pi, *Fluctuations in the New Inflationary Universe*, Phys. Rev. Lett. **49** (1982) 1110–1113.

[19] S. Hawking, *The Development of Irregularities in a Single Bubble Inflationary Universe*, Phys. Lett. **B115** (1982) 295.

[20] K. Dimopoulos and D. H. Lyth, *Models of inflation liberated by the curvaton hypothesis*, Phys. Rev. **D69** (2004) 123509, [hep-ph/0209180].

[21] N. Bartolo, E. Komatsu, S. Matarrese, and A. Riotto, *Non-Gaussianity from inflation: Theory and observations*, Phys. Rept. **402** (2004) 103–266, [astro-ph/0406398].

[22] A. Liddle, *An Introduction to Modern Cosmology*, Wiley, 2 ed., May, 2003.

[23] C. Bennett, A. Banday, K. Gorski, G. Hinshaw, P. Jackson, et al., *Four year COBE DMR cosmic microwave background observations: Maps and basic results*, Astrophys. J. **464** (1996) L1–L4, [astro-ph/9601067].

[24] D. Spergel et al., *Wilkinson Microwave Anisotropy Probe (WMAP) three year results: implications for cosmology*, Astrophys. J. Suppl. **170** (2007) 377, [astro-ph/0603449].

[25] E. Komatsu et al., *Five-Year Wilkinson Microwave Anisotropy Probe (WMAP) Observations: Cosmological Interpretation*, Astrophys. J. Suppl. **180** (2009) 330–376, [arXiv:0803.0547].

[26] A. Friedman, *Über die krümmung des raumes*, Zeitschrift für Physik A Hadrons and Nuclei **10** (1922) 377–386, 10.1007/BF01332580.

[27] C. W. Misner, K. S. Thorne, J. A. Wheeler, J. Wheeler, and K. Thorne, *Gravitation (Physics Series)*, W. H. Freeman, first edition ed., Sept., 1973.

[28] S. Weinberg, *Cosmology*, Oxford University Press, USA, Apr., 2008.

[29] S. Dodelson, *Modern Cosmology*, Academic Press, Elsevier Science, 2003.

[30] D. H. Lyth and A. R. Liddle, *The Primordial Density Perturbation*, Cambridge University Press, 2009.

[31] A. Albrecht and P. J. Steinhardt, *Cosmology for Grand Unified Theories with Radiatively Induced Symmetry Breaking*, Phys.Rev.Lett. **48** (1982) 1220–1223.

[32] V. F. Mukhanov, H. Feldman, and R. H. Brandenberger, *Theory of cosmological perturbations. Part 1. Classical perturbations. Part 2. Quantum theory of perturbations. Part 3. Extensions*, Phys. Rept. **215** (1992) 203–333.

[33] V. Mukhanov and S. Winitzki, *Introduction to Quantum Effects in Gravity*, Cambridge University Press, June, 2007.

[34] T. Bunch and P. Davies, *Quantum Field Theory in de Sitter Space: Renormalization by Point Splitting*, Proc. Roy. Soc. Lond. **A360** (1978) 117–134.

[35] M. Boas, *Mathematical methods in the physical sciences*, Wiley, Hoboken, NJ, 2006.

[36] A. Riotto, *Inflation and the theory of cosmological perturbations*, hep-ph/0210162.

[37] R. Allahverdi, R. Brandenberger, F.-Y. Cyr-Racine, and A. Mazumdar, *Reheating in Inflationary Cosmology: Theory and Applications*, Ann. Rev. Nucl. Part. Sci. **60** (2010) 27–51, [arXiv:1001.2600].

[38] A. V. Frolov, *Non-linear Dynamics and Primordial Curvature Perturbations from Preheating*, Class. Quant. Grav. **27** (2010) 124006, [arXiv:1004.3559].

[39] G. N. Felder, L. Kofman, and A. D. Linde, *Instant preheating*, Phys. Rev. **D59** (1999) 123523, [hep-ph/9812289].

[40] G. N. Felder, J. Garcia-Bellido, P. B. Greene, L. Kofman, A. D. Linde, et al., *Dynamics of symmetry breaking and tachyonic preheating*, Phys. Rev. Lett. **87** (2001) 011601, [hep-ph/0012142].

[41] T. Prokopec and T. G. Roos, *Lattice study of classical inflaton decay*, Phys. Rev. **D55** (1997) 3768–3775, [hep-ph/9610400].

[42] G. Floquet, *Sur les équations différentielles linéaires à coefficients périodiques*, Annales de l'École Normale Supérieure **12** (1883) 47–88.

[43] L. Kofman, A. D. Linde, and A. A. Starobinsky, *Towards the theory of reheating after inflation*, Phys. Rev. **D56** (1997) 3258–3295, [hep-ph/9704452].

[44] A. R. Liddle and L. A. Urena-Lopez, *Inflation, dark matter and dark energy in the string landscape*, Phys. Rev. Lett. **97** (2006) 161301, [astro-ph/0605205].

[45] A. R. Liddle, C. Pahud, and L. A. Urena-Lopez, *Triple unification of inflation, dark matter, and dark energy using a single field*, Phys. Rev. **D77** (2008) 121301, [arXiv:0804.0869].

[46] D. I. Podolsky, G. N. Felder, L. Kofman, and M. Peloso, *Equation of state and beginning of thermalization after preheating*, Phys. Rev. **D73** (2006) 023501, [hep-ph/0507096].

[47] E. Lifshitz, *On the Gravitational stability of the expanding universe*, J. Phys.(USSR) **10** (1946) 116.

[48] J. M. Bardeen, *Gauge Invariant Cosmological Perturbations*, Phys. Rev. **D22** (1980) 1882–1905.

[49] K. A. Malik, *Cosmological perturbations in an inflationary universe*, PhD thesis, University of Portsmouth, 2001, `astro-ph/0101563`.

[50] S. Matarrese, S. Mollerach, and M. Bruni, *Second order perturbations of the Einstein-de Sitter universe*, Phys. Rev. **D58** (1998) 043504, [`astro-ph/9707278`].

[51] U. Seljak and M. Zaldarriaga, *A Line of sight integration approach to cosmic microwave background anisotropies*, Astrophys. J. **469** (1996) 437–444, [`astro-ph/9603033`].

[52] C. Gordon, D. Wands, B. A. Bassett, and R. Maartens, *Adiabatic and entropy perturbations from inflation*, Phys.Rev. **D63** (2001) 023506, [`astro-ph/0009131`].

[53] K. A. Malik, D. Wands, and C. Ungarelli, *Large scale curvature and entropy perturbations for multiple interacting fluids*, Phys. Rev. **D67** (2003) 063516, [`astro-ph/0211602`].

[54] K. A. Malik and D. Wands, *Adiabatic and entropy perturbations with interacting fluids and fields*, JCAP **0502** (2005) 007, [`astro-ph/0411703`].

[55] H. Kodama and M. Sasaki, *Cosmological Perturbation Theory*, Prog. Theor. Phys. Suppl. **78** (1984) 1–166.

[56] M. Bruni, S. Matarrese, S. Mollerach, and S. Sonego, *Perturbations of space-time: Gauge transformations and gauge invariance at second order and beyond*, Class. Quant. Grav. **14** (1997) 2585–2606, [`gr-qc/9609040`].

[57] R. Sachs and A. Wolfe, *Perturbations of a cosmological model and angular variations of the microwave background*, Astrophys.J. **147** (1967) 73–90.

[58] A. D. Linde and V. F. Mukhanov, *Nongaussian isocurvature perturbations from inflation*, Phys. Rev. **D56** (1997) 535–539, [`astro-ph/9610219`].

[59] K. Enqvist and M. S. Sloth, *Adiabatic CMB perturbations in pre - big bang string cosmology*, Nucl. Phys. **B626** (2002) 395–409, [`hep-ph/0109214`].

[60] D. H. Lyth and D. Wands, *Generating the curvature perturbation without an inflaton*, Phys. Lett. **B524** (2002) 5–14, [hep-ph/0110002].

[61] N. Bartolo and A. R. Liddle, *The Simplest curvaton model*, Phys. Rev. **D65** (2002) 121301, [astro-ph/0203076].

[62] T. Moroi and T. Takahashi, *Cosmic density perturbations from late decaying scalar condensations*, Phys. Rev. **D66** (2002) 063501, [hep-ph/0206026].

[63] K. Dimopoulos, G. Lazarides, D. Lyth, and R. Ruiz de Austri, *Curvaton dynamics*, Phys. Rev. **D68** (2003) 123515, [hep-ph/0308015].

[64] T. Moroi and T. Takahashi, *Effects of cosmological moduli fields on cosmic microwave background*, Phys. Lett. **B522** (2001) 215–221, [hep-ph/0110096].

[65] G. N. Felder and I. Tkachev, *LATTICEEASY: A Program for lattice simulations of scalar fields in an expanding universe*, Comput. Phys. Commun. **178** (2008) 929–932, [hep-ph/0011159].

[66] A. V. Frolov, *DEFROST: A New Code for Simulating Preheating after Inflation*, JCAP **0811** (2008) 009, [arXiv:0809.4904].

[67] R. Easther, H. Finkel, and N. Roth, *PSpectRe: A Pseudo-Spectral Code for (P)reheating*, JCAP **1010** (2010) 025, [arXiv:1005.1921].

[68] Z. Huang, *The Art of Lattice and Gravity Waves from Preheating*, Phys. Rev. **D83** (2011) 123509, [arXiv:1102.0227].

[69] R. G. Belleman, J. Bedorf, and S. P. Zwart, *High Performance Direct Gravitational N-body Simulations on Graphics Processing Units. 2. An implementation in CUDA*, New Astron. **13** (2008) 103–112, [arXiv:0707.0438].

[70] R. J. Brunner, V. V. Kindratenko, and A. D. Myers, *Developing and Deploying Advanced Algorithms to Novel Supercomputing Hardware*, in *Proceedings of NASA Science Technology Conference - NSTC'07*, 2007, arXiv:0711.3414.

[71] S. P. Zwart, S. McMillan, S. Harfst, D. Groen, and M. Fujii, *A multiphysics and multiscale software environment for modeling astrophysical systems*, New Astron. **14** (2009) 369–378, [arXiv:0807.1996].

[72] K.-I. Ishikawa, *Recent algorithm and machine developments for lattice QCD*, PoS **LATTICE2008** (2008) 013, [arXiv:0811.1661].

[73] T. Szalay, V. Springel, and G. Lemson, *GPU-Based Interactive Visualization of Billion Point Cosmological Simulations*, Nov., 2008, arXiv:0811.2055, Presented at 2008 Microsoft eScience Workshop.

[74] V. Anselmi, G. Conti, and F. Di Renzo, *GPU computing for 2-d spin systems: CUDA vs OpenGL*, PoS **LATTICE2008** (2008) 024, [arXiv:0811.2111].

[75] E. B. Ford, *Parallel Algorithm for Solving Kepler's Equation on Graphics Processing Units: Application to Analysis of Doppler Exoplanet Searches*, New Astron. **14** (2009) 406–412, [arXiv:0812.2976].

[76] S. Ord, L. Greenhill, R. Wayth, D. Mitchell, K. Dale, et al., *GPUs for data processing in the MWA*, in *Proceedings of the Astronomical Data Analysis Software and Systems (ADASS) XVII conference*, 2009, arXiv:0902.0915.

[77] E. Gaburov, S. Harfst, and S. Portegies Zwart, *SAPPORO: A way to turn your graphics cards into a GRAPE-6*, New Astronomy **14** (Oct., 2009) 630–637, [arXiv:0902.4463].

[78] V. Demchik and A. Strelchenko, *Monte Carlo simulations on Graphics Processing Units*, arXiv:0903.3053.

[79] S. K. Chung, L. Wen, D. Blair, K. Cannon, and A. Datta, *Application of Graphics Processing Units to Search Pipeline for Gravitational Waves from Coalescing Binaries of Compact Objects*, Class. Quant. Grav. **27** (2010) 135009, [arXiv:0906.4175].

[80] H.-Y. Schive, Y.-C. Tsai, and T. Chiueh, *GAMER: a GPU-Accelerated Adaptive Mesh Refinement Code for Astrophysics*, Astrophys. J. Suppl. **186** (2010) 457–484, [arXiv:0907.3390].

[81] P. B. Jonsson and J. Primack, *Accelerating Dust Temperature Calculations with Graphics Processing Units*, New Astron. **15** (2010) 509–514, [arXiv:0907.3768].

[82] D. Groen, S. Harfst, and S. Portegies Zwart, *The living application: a self-organizing system for complex grid tasks*, International Journal of High Performance Computing Applications **24** (2010), no. 2 185–193, [http://hpc.sagepub.com/content/24/2/185.full.pdf+html].

[83] N. Nakasato, *Oct-tree Method on GPU*, arXiv:0909.0541, Poster paper presented at SC09.

[84] G. Khanna and J. McKennon, *An Exploration of CUDA and CBEA for a gravitational wave source-modelling application*, in *Proceedings of Parallel and Distributed Computing and Systems (PDCS 2009)*.

[85] K. Hagiwara, J. Kanzaki, N. Okamura, D. Rainwater, and T. Stelzer, *Calculation of HELAS amplitudes for QCD processes using graphics processing unit (GPU)*, Eur. Phys. J. **C70** (2010) 513–524, [arXiv:0909.5257].

[86] R. Capuzzo-Dolcetta, *Supercomputing and stellar dynamics*, arXiv:0909.0879, Invited talk to the 2009 general Conference of the Societa' Astronomica Italiana.

[87] S. Banerjee, H. Baumgardt, and P. Kroupa, *Stellar-mass black holes in star clusters: implications for gravitational wave radiation*, Monthly Notices of the Royal Astronomical Society **402** (Feb., 2010) 371–380, [arXiv:0910.3954].

[88] P. Wang, T. Abel, and R. Kaehler, *Adaptive Mesh Fluid Simulations on GPU*, New Astron. **15** (2010) 581–589, [arXiv:0910.5547].

[89] M. Januszewski and M. Kostur, *Accelerating numerical solution of stochastic differential equations with CUDA*, Computer Physics Communications **181** (Jan., 2010) 183–188, [arXiv:0903.3852].

[90] *NVIDIA CUDA Compute Unified Device Architecture - Programming Guide*, 2007.

[91] J. Sanders and E. Kandrot, *CUDA by Example: An Introduction to General-Purpose GPU Programming*, Addison-Wesley Professional, 1 ed., July, 2010.

[92] A. V. Frolov, private communication.

[93] B. Leimkuhler and S. Reich, *Simulating Hamiltonian dynamics* Cambridge monographs on applied and computational mathematics, 14, Cambridge University Press, 2004.

[94] M. Patra and M. Karttunen, *Stencils with isotropic discretization error for differential operators*, Numerical Methods for Partial Differential Equations **22** (2006), no. 4 936–953.

[95] S. Y. Khlebnikov and I. Tkachev, *Classical decay of inflaton*, Phys. Rev. Lett. **77** (1996) 219–222, [hep-ph/9603378].

[96] J. Salmon, *Generation of Correlated and Constrained Gaussian Stochastic Processes for N-Body Simulations*, Astrophys. J. **460** (Mar., 1996) 59.

[97] U.-L. Pen, *Generating cosmological Gaussian random fields*, Astrophys. J. **490** (1997) L127–L130, [astro-ph/9709261].

[98] R. I. McLachlan and G. R. W. Quispel, *Splitting methods*, Acta Numerica **11** (2002) 341–434, [http://journals.cambridge.org/article_S0962492902000053].

[99] P. Micikevicius, *3d finite difference computation on gpus using cuda*, in *Proceedings of 2nd Workshop on General Purpose Processing on Graphics Processing Units*, GPGPU-2, (New York, NY, USA), pp. 79–84, ACM, 2009.

[100] E. Komatsu et al., *First year Wilkinson Microwave Anisotropy Probe (WMAP) observations: tests of gaussianity*, Astrophys. J. Suppl. **148** (2003) 119–134, [astro-ph/0302223].

[101] C. T. Byrnes and K.-Y. Choi, *Review of local non-Gaussianity from multi-field inflation*, Adv. Astron. **2010** (2010) 724525, [arXiv:1002.3110].

[102] S. Mollerach and S. Matarrese, *Cosmic microwave background anisotropies from second order gravitational perturbations*, Phys. Rev. **D56** (1997) 4494–4502, [astro-ph/9702234].

[103] D. H. Lyth and Y. Rodriguez, *The Inflationary prediction for primordial non-Gaussianity*, Phys. Rev. Lett. **95** (2005) 121302, [astro-ph/0504045].

[104] E. Komatsu, *The pursuit of non-gaussian fluctuations in the cosmic microwave background*, PhD thesis, Tohoku University, 2001, astro-ph/0206039.

[105] K. Enqvist, A. Jokinen, A. Mazumdar, T. Multamäki, and A. Väihkönen, *Non-Gaussianity from preheating*, Phys. Rev. Lett. **94** (2005) 161301, [astro-ph/0411394].

[106] K. Enqvist, A. Jokinen, A. Mazumdar, T. Multamäki, and A. Väihkönen, *Non-Gaussianity from instant and tachyonic preheating*, JCAP **0503** (2005) 010, [hep-ph/0501076].

[107] A. Jokinen and A. Mazumdar, *Very large primordial non-gaussianity from multi-field: application to massless preheating*, JCAP **0604** (2006) 003, [astro-ph/0512368].

[108] A. Chambers and A. Rajantie, *Lattice calculation of non-Gaussianity from preheating*, Phys. Rev. Lett. **100** (2008) 041302, [arXiv:0710.4133].

[109] A. Chambers and A. Rajantie, *Non-Gaussianity from massless preheating*, JCAP **0808** (2008) 002, [arXiv:0805.4795].

[110] J. R. Bond, A. V. Frolov, Z. Huang, and L. Kofman, *Non-Gaussian Spikes from Chaotic Billiards in Inflation Preheating*, Phys. Rev. Lett. **103** (2009) 071301, [arXiv:0903.3407].

[111] A. Chambers, S. Nurmi, and A. Rajantie, *Non-Gaussianity from resonant curvaton decay*, JCAP **1001** (2010) 012, [arXiv:0909.4535].

[112] D. Wands, K. A. Malik, D. H. Lyth, and A. R. Liddle, *A New approach to the evolution of cosmological perturbations on large scales*, Phys. Rev. **D62** (2000) 043527, [astro-ph/0003278].

[113] D. S. Salopek and J. R. Bond, *Nonlinear evolution of long-wavelength metric fluctuations in inflationary models*, Phys. Rev. D **42** (Dec, 1990) 3936–3962.

[114] R. Micha and I. I. Tkachev, *Relativistic turbulence: A Long way from preheating to equilibrium*, Phys. Rev. Lett. **90** (2003) 121301, [hep-ph/0210202].